Available online at www.sciencedirect.com
SCIENCE DIRECT®
Chemical Physics 284 (2002) 139–168
Chemical Physics
www.elsevier.com/locate/chemphys

Non-Debye dielectric relaxation in complex materials

Yuri Feldman *, Alexander Puzenko, Yaroslav Ryabov [1]

Department of Applied Physics, School of Applied Science, The Hebrew University of Jerusalem, Givat-Ram, 91904 Jerusalem, Israel

Received 12 November 2001

Abstract

The paper considers several examples of non-Debye dielectric response in complex heterogeneous media. The percolation phenomenon and Cole–Cole relaxation in disordered matter are discussed in detail. The proposed models are illustrated by different sample systems: ionic microemulsions, porous glasses, porous silicon, polymer–water mixtures, and polymer–microcomposite materials. The models enable us to establish the relationship between the parameters of dielectric relaxation broadening, structural properties of the media and transport features of charge carriers in the considered systems. In addition, the origins of "strange kinetic" phenomena were discussed based on statistical physics and fractional time evolution ideas.

1. Introduction

Recent years have witnessed extensive research of soft condensed matter physics to investigate the structure, dynamics, and macroscopic behavior of complex systems (*CS*). *CS* are a very broad and general class of materials that are typically non-crystalline. Polymers, biopolymers, colloid systems (emulsions and microemulsions), biological cells, porous materials, and liquid crystals can be considered as *CS*. All these systems exhibit a common feature: the new "*mesoscopic*" length scale, intermediate between molecular and macroscopic. The dynamic processes occurring in *CS* include different length and time scales. Both fast and ultra-slow molecular rearrangements take place within the microscopic, mesoscopic and macroscopic organization of the systems.

A common theme in *CS* is that while the materials are disordered at the molecular scale and homogeneous at the macroscopic scale, they usually possess a certain amount of order at an intermediate, so-called mesoscopic, scale due to a delicate balance of interaction and thermal effects. Simple exponential relaxation law and the classical model of Brownian diffusion cannot describe the relaxation phenomena and kinetics in such materials. This kind of non-exponential relaxation behavior and anomalous diffusion phenomena is today called "strange kinetics" [1].

Generally, the complete characterization of these relaxation behaviors requires the use of a variety of techniques in order to span the relevant

* Corresponding author. Tel.: +972-2-6586187; fax: +972-2-5663878.
E-mail address: yurif@vms.huji.ac.il (Y. Feldman).
[1] Permanent address: Institute for Mechanics and Engineering, 420111 Kazan, Russia.

0301-0104/02/$ - see front matter
PII: S0301-0104(02)00545-1

ranges in frequency. In this regard, the Dielectric Spectroscopy (*DS*) has its own advantages. The modern *DS* technique may overlap extremely wide frequency (10^{-6} to 10^{11} Hz) and temperature (−170 to +500°C) ranges [2–4]. *DS* is especially sensitive to intermolecular interactions and is able to monitor cooperative processes at the molecular level. Therefore, this method is more appropriate than any other to monitor such different scales of molecular motion. It provides a link between the investigation – via molecular spectroscopy – of the properties of the individual constituents of the complex material and the characterization of its bulk properties. The recent successful developments of the Time Domain Dielectric Spectroscopy (*TDDS*) method and Broadband Dielectric Spectroscopy (*BDS*) have radically changed the attitude towards *DS*; it is now recognized as an effective investigative tool for research on solids and liquids at macroscopic, microscopic and mesoscopic levels.

It is known that when an external field is applied to the dielectric, polarization of the material reaches its equilibrium value, not instantly, but over a period of time. By analogy, when the field is removed suddenly, the polarization decay caused by thermal motion follows the same law as the relaxation or decay function of dielectric polarization $\phi(t)$:

$$\phi(t) = \frac{\boldsymbol{P}(t)}{\boldsymbol{P}(0)}, \tag{1.1}$$

where $\boldsymbol{P}$ is a polarization vector of a sample unit. The relationship for the dielectric displacement vector $\boldsymbol{D}(t)$ in the case of time dependent fields may be written as follows [5,6]:

$$\boldsymbol{D}(t) = \varepsilon_\infty \boldsymbol{E}(t) + \int_{-\infty}^{t} \frac{\mathrm{d}\Phi(t')}{\mathrm{d}t'} \boldsymbol{E}(t-t')\,\mathrm{d}t'. \tag{1.2}$$

In (1.2) $\boldsymbol{D}(t) = \varepsilon_0 \boldsymbol{E}(t) + \boldsymbol{P}(t)$, where ε_0 is the dielectric permittivity of free space, ε_∞ is the high-frequency limit of the complex dielectric permittivity $\varepsilon^*(\omega)$, and $\Phi(t)$ is the dielectric response function $\Phi(t) = (\varepsilon_s - \varepsilon_\infty)[1 - \phi(t)]$, where ε_s is the low-frequency limit of the complex dielectric permittivity. The complex dielectric permittivity $\varepsilon^*(\omega)$ is connected with the relaxation function by a very simple relationship [5,6]

$$\frac{\varepsilon^*(\omega) - \varepsilon_\infty}{\varepsilon_s - \varepsilon_\infty} = \hat{L}\left[-\frac{\mathrm{d}}{\mathrm{d}t}\phi(t) \right], \tag{1.3}$$

where $\hat{L}$ is the operator of the Laplace transform, which is defined for the arbitrary time-dependent function $f(t)$ as

$$\hat{L}[f(t)] = \int_0^\infty \mathrm{e}^{-pt} f(t)\,\mathrm{d}t, \tag{1.4}$$

where $p = i\omega$ and $i$is the imaginary unity.
If

$$\phi(t) = \exp(-t/\tau_m), \tag{1.5}$$

where τ_m represents the characteristic dielectric relaxation time, then the relation first obtained by Debye is true for the frequency domain [5–7]

$$\frac{\varepsilon^*(\omega) - \varepsilon_\infty}{\varepsilon_s - \varepsilon_\infty} = \frac{1}{1 + i\omega\tau_m}. \tag{1.6}$$

For most of the systems being studied, the relationship above does not sufficiently describe the experimental results. This causes the necessity for empirical relationships, which formally take into account the distribution of the relaxation times. In the most general way such non-Debye dielectric behavior can be described in terms of a continuous distribution of relaxation times, $g(\tau)$ [6]. This implies that the complex dielectric permittivity can be presented as follows:

$$\frac{\varepsilon^*(\omega) - \varepsilon_\infty}{\varepsilon_s - \varepsilon_\infty} = \int_0^\infty \frac{g(\tau)}{1 + i\omega\tau}\,\mathrm{d}\tau, \tag{1.7}$$

where distribution function $g(\tau)$ satisfies the normalization condition

$$\int_0^\infty g(\tau)\,\mathrm{d}\tau = 1. \tag{1.8}$$

The corresponding expression for the decay function is

$$\phi(t) = \int_0^\infty g(\tau)\mathrm{e}^{-t/\tau}\,\mathrm{d}\tau. \tag{1.9}$$

It must be clearly understood that by virtue of the univalent relationship (1.3) between frequency and time representation the $g(\tau)$ calculation does not by itself provide anything more than another way of describing the dynamic behavior of the dielectric in time domain [8]. Moreover, such a

calculation is a mathematically ill-posed problem [9,10], which leads to additional mathematical difficulties. On some occasions, a frequency data analysis can provide a clearer physical interpretation [10,11]. In most cases of non-Debye dielectric spectrums the data have been described by the so-called Havriliak–Negami (*HN*) relationship [6,7,12]

$$\varepsilon^*(\omega) = \varepsilon_\infty + \frac{\varepsilon_s - \varepsilon_\infty}{\left[1 + (i\omega\tau_m)^\alpha\right]^\beta}, \quad 0 < \alpha, \beta < 1. \tag{1.10}$$

Here α and β are empirical exponents. The specific case $\alpha = 1, \beta = 1$ gives the Debye relaxation law, $\beta = 1, \alpha \neq 1$ corresponds to the so-called Cole–Cole (*CC*) equation [13], whereas the case $\alpha = 1, \beta \neq 1$, corresponds to the Cole–Davidson (*CD*) formula [14].

Sometimes in the case of superposition of relaxation processes with dc and ac conductivities the high and low frequency asymptotic forms are usually assigned to Jonscher power-law wings $(i\omega\tau_i)^{(n_i-1)}$ (n_i is a Jonscher stretch parameter, and τ_i is the correspondent characteristic relaxation time) [15,16]. Notice that the real part $\varepsilon'(\omega)$ of the complex dielectric permittivity is proportional to the imaginary part $\sigma''(\omega)$ of the complex ac-conductivity $\sigma^*(\omega)$, $\varepsilon'(\omega) \propto -\sigma''(\omega)/\omega$, and the dielectric losses $\varepsilon''(\omega)$ is proportional to the real part $\sigma'(\omega)$ of the ac conductivity, $\varepsilon''(\omega) \propto \sigma'(\omega)/\omega$. The latter arises from the Jonscher term and has the form, $\sigma'(\omega) \propto \omega^{\mu_j}$, which has been termed "*universal*" due to its appearance in many types of disordered systems [17,18]. Progress has been made recently in understanding the physical significance of the empirical parameters α, β and exponents of Jonscher wings [19–22].

An alternative approach to *DS* study is to examine the dynamic molecular properties of a substance directly in time domain. Relation (1.3) shows that the equivalent information on the dielectric relaxation properties of a sample being tested can be obtained in both frequency and time domains.

In the linear response approximation, the fluctuations of polarization caused by thermal motion are the same as for the macroscopic reconstruction induced by the electric field [23,24]. Thus, one can equate the relaxation function $\phi(t)$ and the macroscopic dipole correlation function (*DCF*) $\Psi(t)$ as follows:

$$\phi(t) \cong \Psi(t) = \frac{\langle \boldsymbol{M}(0)\boldsymbol{M}(t)\rangle}{\langle \boldsymbol{M}(0)\boldsymbol{M}(0)\rangle}, \tag{1.11}$$

where $\boldsymbol{M}(t)$ is the macroscopic fluctuating dipole moment of the sample volume unit, which is equal to the vector sum of all the molecular dipoles. The rate and laws governing the *DCF* $\Psi(t)$ are directly related to the structural and kinetic properties of the sample and characterize the macroscopic properties of the system under study. Thus, the experimental function $\Phi(t)$ and hence $\phi(t)$ or $\Psi(t)$ can be used to obtain information on the dynamic properties of the dielectric under investigation. The dielectric relaxation of many complex systems deviates from the classical exponential Debye pattern (1.5) and can be described by the Kohlrausch–Williams–Watts (*KWW*) law or the "*stretched exponential law*" [25,26]

$$\phi(t) = \exp\left\{-\left(\frac{t}{\tau_m}\right)^\nu\right\} \tag{1.12}$$

with a characteristic relaxation time τ_m and empirical exponent $0 < \nu \leqslant 1$. The *KWW* decay function can be considered as a generalization of Eq. (1.5) that becomes Debye law when $\nu = 1$. Another common experimental observation of *DCF* is the asymptotic power law [15,16],

$$\phi(t) = A\left(\frac{t}{\tau_1}\right)^{-\mu}, \quad t \geqslant \tau_1, \tag{1.13}$$

with amplitude A, exponent $\mu > 0$ and a characteristic time τ_1 which is associated with the effective relaxation time of the microscopic structural unit. This relaxation power law is sometimes referred to the literature to describing anomalous transport when the mean square displacement does not obey the linear dependency $\langle R^2\rangle \sim t$. Instead, it is proportional to some power of time $\langle R^2\rangle \sim t^\gamma$ $(0 < \gamma < 2)$ [27–29]. In this case, the parameter τ_1 is an effective relaxation time, which corresponds to the charge carrier motion of an average displacement equal to the size of the minimal structural unit. A number of approaches exist to describe such kinetic processes: Fokker–Planck equation [30], propagator representation [31],

different models of dc and ac conductivities [17,22], etc.

In frequency domain, Jonscher power-law wings evaluated by ac-conductivity measurements. In particular, it treat to anomalous diffusion as a random walk in fractal geometry or as a thermally activated hopping transport mechanism [32]. An example of a phenomenological decay function that has different short- and long-time asymptotic forms (with the different characteristic times) can be presented as follows [33,34]:

$$\phi(t) = A\left(\frac{t}{\tau_1}\right)^{-\mu} \exp\left\{-\left(\frac{t}{\tau_m}\right)^{\nu}\right\}. \qquad (1.14)$$

This function is the product of *KWW* and power-law dependencies. The relaxation law (1.14) in time domain and the *HN* law (1.10) in frequency domain are rather generalized representations that lead to the known dielectric relaxation laws. The fact that these functions have the power-law asymptotic inspires numerous attempts to establish a relationship between their various parameters [11,35]. In this regard, the exact relationship between the parameters of (1.14) and the *HN* law should be a consequence of the Laplace transform according to Eq. (1.3) [6,8]. However, there is currently no concrete proof that this is indeed so. Thus, the relationship between the parameters of decay function (1.14) and the *HN* law seems to be valid only asymptotically.

In this contribution, we will to consider the experimental evidence of non-Debye dielectric responses in several complex disordered systems such as microemulsions, porous glasses, porous silicon, aqueous solutions of polymers and composite materials. The purpose of this paper is to describe how *DS* can be utilized to investigate complex systems to obtain information regarding molecular mobility and the mesoscale structure from the dielectric data.

2. Dielectric relaxation in ionic microemulsions near the percolation threshold

Microemulsions are thermodynamically stable, clear fluids composed of oil, water, surfactant, and sometimes a co-surfactant. They have been widely investigated during recent years because of their numerous practical applications. The chemical structure of surfactants may be low-molecular weight as well as polymeric, with non-ionic or ionic components [36–38]. In the case of an oil-continuous water in oil (*W/O*) microemulsion, at low concentrations of the dispersed phase, the structure is that of spherical water droplets surrounded by a monomolecular layer of surfactant molecules whose hydrophobic tails are oriented towards the continuous oil phase [38–41].

The structure of the microemulsion depends on the interactions between droplets. In the case of repulsive interactions, the collisions of the droplets are short and no overlapping occurs between their interfaces. However, if the interactions are attractive, transient droplet clusters are formed. The number of such clusters increases when the water fraction, the temperature, the pressure, or the ratio of water to surfactant is increased, leading to a percolation in the system [42–48]. The percolation behavior is manifested by the rapid increase in the dc-electrical conductivity σ and the static dielectric permittivity ε_s as system approaches the percolation threshold (Fig. 1).

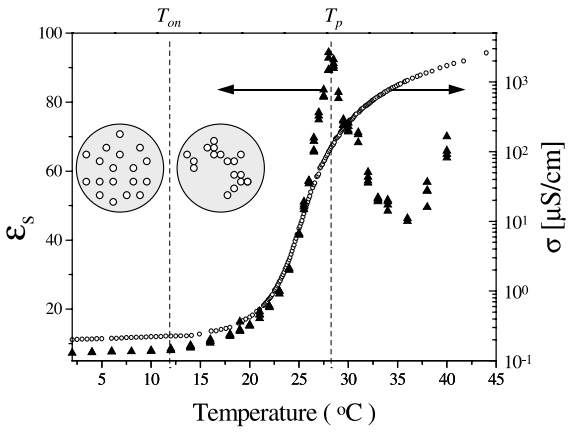

Fig. 1. The percolation behavior in *AOT*–water–decane microemulsion (17.5:21.3:61.2 vol%) is manifested by the temperature dependencies of the static dielectric permittivity ε_s (▲ left axis) and conductivity σ (○ right axis). T_{on} is the temperature of the percolation onset; T_p is the temperature of the percolation threshold. Insets are schematic presentations of the microemulsion structure far below percolation and at the percolation onset. (From [51]. With permission from Elsevier Science B.V.)

The dielectric relaxation properties in a sodium bis(2-ethylhexyl) sulfosuccinate (*AOT*)–water–decane microemulsion near the percolation temperature threshold have been investigated recently in the broad temperature region [43,44,49]. The dielectric measurements of ionic microemulsions were carried out using the *TDDS* in a time window of $\sim$1 μs.

It was found that the system exhibits a complex non-exponential relaxation behavior that is strongly temperature dependent (Fig. 2). An interpretation of the results was done in the framework of the dynamic percolation model [50]. According to this model, near the percolation threshold, in addition *to the fast relaxation* related to the dynamics of droplet components ($\tau_1 \cong 1$ ns) [51], there are at least two much longer characteristic time scales. *The longest process* has a characteristic relaxation time greater than a few microseconds and is associated with the rearrangements of the typical percolation cluster. The temporal window of the intermediate process is a function of temperature. This *intermediate process* reflects the *cooperative relaxation phenomenon* associated with the transport of charge carriers along the percolation cluster [50,52,53]. Thus, due to the cooperative nature of relaxation, the *DCF* decay behavior contains information regarding the transient cluster morphology at the mesoscale that reflects the dynamical character of percolation.

The type of the relaxation law seen in time domain is strongly dependent on the distance from the percolation threshold. Fig. 3 shows in log–log coordinates that at the percolation onset temperature ($\sim$14 °C) the relaxation follows a fractional power law: $\Psi(t) \sim (t/\tau_1)^{-\mu}$. By the same token, in the coordinates $\log \Psi$ versus $\log(t/\tau_1)$ in the close vicinity of the percolation threshold $T_p = 26.5$ °C, the relaxation law changes from a power law to stretched exponential behavior, i.e., $\Psi(t) \sim \exp[-(t/\tau_m)^{\nu}]$ (see Fig. 4). In the crossover region

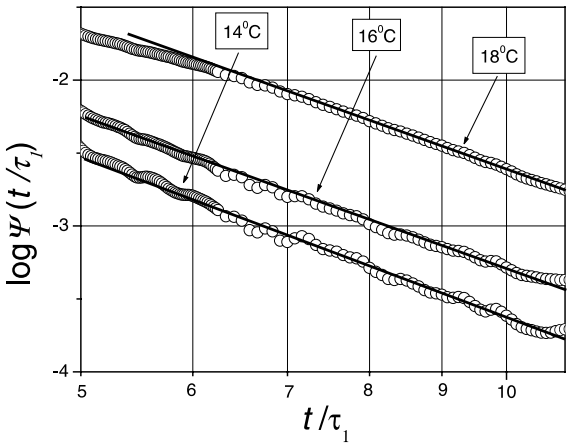

Fig. 3. The dipole correlation function $\psi(t/\tau_1)$ demonstrates the power-law behavior for the temperature region near the percolation onset ($T_{on} = 14$ °C).

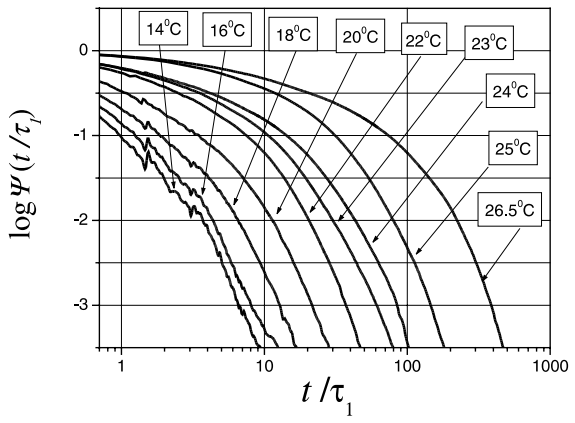

Fig. 2. The dipole correlation function $\psi(t/\tau_1)$ for different temperatures. The percolation threshold temperature $T_p = 26.5$ °C.

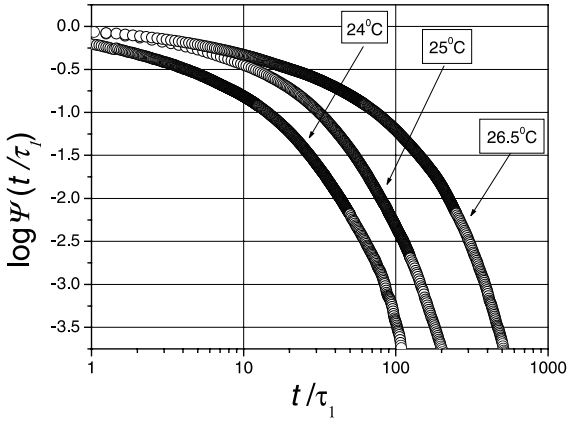

Fig. 4. The dipole correlation function $\psi(t/\tau_1)$ demonstrates *KWW* behavior near the temperature of the percolation threshold ($T_p = 26.5$°C).

the relaxation law is considered to be a product of both the power law and stretched exponential terms described by Eq. (1.14).

The results of the fitting of the experimental dipole correlation functions to Eq. (1.14) are shown in Figs. 5 and 6. One can see (Fig. 5) that the magnitude of the parameter μ decreases to almost zero as the temperature approaches that of the percolation threshold. This effect confirms the statement mentioned above that at the percolation threshold temperature the behavior of the dipole correlation function is of the *KWW* type. The stretched parameter v changes its value from $\sim$0.2 near the percolation onset to $\sim$0.8 in the vicinity of percolation threshold. Notwithstanding the value of v is not equal to zero at percolation onset, note that the stretched exponential term with $v = 0.2$ changes insignificantly in the considerable time interval ($\sim$1 μs) and the decay of *DCF* $\psi(t)$ is governed mainly by the power law.

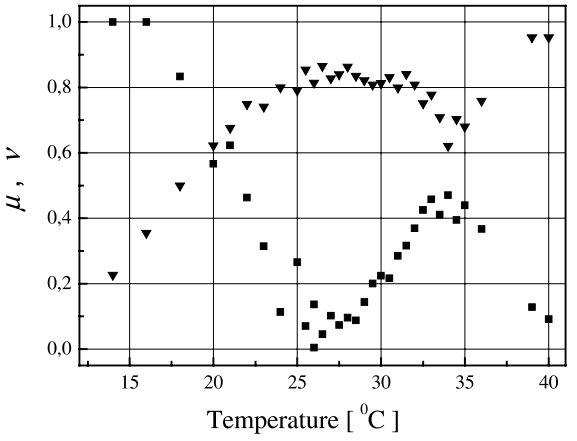

Fig. 5. The temperature dependence of the exponents μ (■) and v (▼) illustrate the transformation of the dipole correlation function $\psi(t/\tau_1)$ from the power-law pattern to the *KWW* behavior at the percolation threshold.

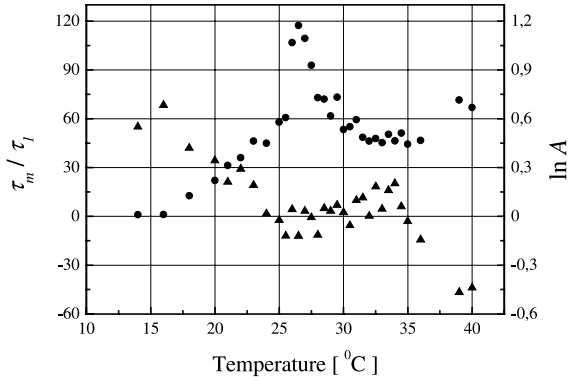

Fig. 6. The temperature dependencies of the parameter τ_m (● left axis) and A (▲ right axis), obtained by the fitting of the relaxation-law (1.14) to the experimental data.

Fig. 6 plots the relaxation time, $\tau_{m/}\tau_1$ and the amplitude A corresponding to the macroscopic relaxation time of the decay function determined by Eq. (1.14). Near the percolation threshold, $\tau_{m/}\tau_1$ exhibits a maximum and reflects the well-known *critical slowing down* effect [54].

A description of the mechanism of the cooperative relaxation in the percolation region was presented recently [44]. In the framework of the theory of cooperative relaxation, it was shown that the macroscopic dipole correlation function $\psi(t)$ of the system is given by

$$\Psi(t) = \exp\left[-\left(\frac{t}{\tau_m}\right)^{v} + B\left(\frac{t}{\tau_1}\right)\right], \tag{2.1}$$

where $\tau_m = \tau_1 W^{-1/v}$, and the microrelaxation time τ_1 describes the charge transfer between two neighboring droplets. The coefficient $W = W[G, N, k, v]$ depends on the scaling parameter k, on the number of cluster self-similarity stages N, and it is a functional of the microscopic relaxation function $G(t)$. The latter describes the elementary act of a charge transfer. Coefficient B is the correction for the *KWW* function at short-time intervals. Parameter v in (2.1) characterizes the cooperative dynamics and structure of the fractal clusters. The relationship between exponent v and the fractal dimension D_s of the recursive fractal is given by [44]

$$D_s = 3v. \tag{2.2}$$

However, the recursive model describes neither the cluster polydispersity (cluster size distribution), nor the relaxation of the individual cluster. Therefore, it is expedient to use the *complementary model* in order to estimate cluster statistics and dynamics in more detail. Such a model might be developed in the framework of the general statistical description.

To describe the percolation phenomenon in ionic microemulsions in terms of the macroscopic *DCF*, the geometrical substrate of the static lattice site percolation model may be used. In this model the statistical ensemble of various size clusters can be presented by the distribution function as follows [55]:

$$w(s,s_m) = C_w \cdot s^{-\Omega} \exp\left(-\frac{s}{s_m}\right). \tag{2.3}$$

Here C_w is the normalization constant, Ω is a scaling exponent of the probability "per lattice site" that the site, chosen randomly, belongs to the s-cluster (a cluster that spans s lattice sites). The value s_m is corresponds to the maximal cluster size [55,56].

We assumed that the mesoscopic dipole correlation functions related to the s-cluster of the geometrical substrate have the simplest exponential form $G[\bar{z},\bar{z}_s(s)] = \exp\lfloor -\bar{z}/\bar{z}_s(s)\rfloor$. Here the dimensionless time $\bar{z} = t/\tau_1$ is normalized by the characteristic relaxation time τ_1, the time required for a charge carrier to move the distance equal to the size of one droplet. Similarly, we introduce the dimensionless time $\bar{z}_s = \tau_s/\tau_1$ where τ_s is the effective correlation time of the s-cluster, and the dimensionless time $\bar{z}_m = \tau_m/\tau_1$. The maximal correlation time τ_m is the effective correlation time correspondent to the maximal cluster s_m. In terms of the random walker problem, it is the time required for a charge carrier to visit all the droplets of a maximal cluster s_m. Thus, the macroscopic *DCF* may be obtained by the averaging procedure [57]

$$\Psi\left[\bar{z},\bar{z}_m(s_m)\right] = \int_1^\infty G\left[\bar{z},\bar{z}_s(s)\right] w(s,s_m)\,\mathrm{d}s. \tag{2.4}$$

Here we present the dynamic percolation process using the classical static site percolation model [54,55]. For this purpose, we must be assume the scaling relationship between τ_m, τ_1 and s_m as follows:

$$\bar{z}_m = \frac{\tau_m}{\tau_1} = s_m^{\eta}, \quad s_m \to \infty, \ \ \eta > 0, \tag{2.5}$$

where $\eta = 1/D_\mathrm{d}$ is an exponent reciprocal to the dynamic fractal dimension D_d. In order to retain the self-similarity of the temporal scaling, the scaling law for the clusters of size $s < s_m$ must be the same as defined by relation (2.5), i.e.

$$\bar{z}_s(s) = s^{\eta}. \tag{2.6}$$

Taking into account relationships (2.5) and (2.6), in the limit of a long time $\bar{z} \gg 1$, the integration of (2.4) may be fulfilled asymptotically by the saddle-point method [33]. The main term of the asymptotic expansion is represented as the multiplication of power and stretch exponential universal relaxation laws:

$$\begin{aligned}\Psi\left(\bar{z}\right) &\cong C\bar{z}^{(1-2\gamma)/[2(1+\eta)]} \exp\left[-Q\cdot\bar{z}^{1/(1+\eta)}\right] \\ &= A\bar{z}^{-\mu}\exp\left[-\left(\frac{\bar{z}}{\bar{z}_m}\right)^{\nu}\right],\end{aligned} \tag{2.7}$$

where

$$Q = (\eta s_m)^{-[\eta/(1+\eta)]}(1+\eta), \quad C = C_w K,$$

and

$$K = \sqrt{\frac{2\pi}{\eta(1+\eta)}}(\eta s_m)^{[\eta+2(1-\Omega)]/2(1+\eta)}.$$

Using (2.7) it is possible to ascertain the relationship between the structural parameters η, Ω, s_m, C_w and the set of fitting phenomenological parameters $\nu, \mu, \bar{z}_m, A$ as follows:

$$\begin{aligned}&\eta = \frac{1}{\nu} - 1, \quad \Omega = \frac{\mu}{\nu} + \frac{1}{2}, \\ &s_m = \frac{1}{\eta}\left(\bar{z}_m\right)^{1/\eta}(1+\eta)^{(1+\eta)/\eta}, \quad C_w = \frac{A}{K}.\end{aligned} \tag{2.8}$$

Thus, the set of structural parameters obtained by fitting using relationship (2.8) can be used to reconstruct the cluster size distribution function $w(s,s_m)$ and to treat the dynamic percolation in ionic microemulsions in terms of the classical static percolation model.

It was shown [57] that the dynamic fractal dimension $D_\mathrm{d} = 1/\eta$ may be associated with the conventional static fractal dimension D_s. From the classical static site percolation model, it is known that D_s can be obtained from the spatial scaling

$$(L/l)^{D_\mathrm{s}} \propto s_m. \tag{2.9}$$

Here L is the macroscopic linear lattice size related to the distance between the internal and external

electrodes of the cylindrical sample cell and l is the linear size of the microdroplet (diameter) in the actual experimental condition [57]. In order to establish the relationship between D_s and D_d it is helpful to introduce the dimensionless coefficient associated with the macroscopic spatial and time scales of the system as follows:

$$\Theta = \frac{(\tau_m/\tau_1)}{(L/l)}.$$

The static fractal dimension can then be calculated from the dynamic fractal dimension using the following formula [57]:

$$D_{\mathrm{s}} = \frac{D_{\mathrm{d}}}{1 - D_{\mathrm{d}} \frac{\ln \Theta}{\ln s_m}}. \tag{2.10}$$

For the actual experimental setup, where $L = 2 \times 10^3$ [58], and $l = 5 \times 10^{-9}$ [43], the non-dimensional lattice size is equal to $L/l = 4 \times 10^5$. Fig. 7 shows the temperature dependencies of the static fractal dimensions of the maximal cluster. Note that at percolation temperature the value of the static fractal dimension D_{s} is extremely close to the classical value 2.53 for a three-dimensional lattice in the static site percolation model [54]. Moreover, the temperature dependence of the stretch parameter v (see Fig. 7) confirms the validity of our previous result (see Eq. (2.2)) $D_{\mathrm{s}} = 3v$ for the percolation cluster [44].

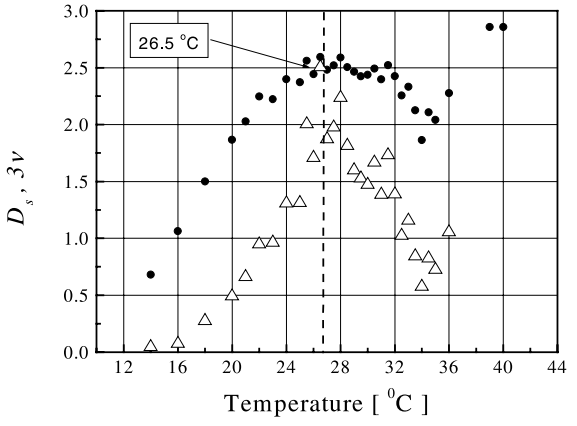

Fig. 7. The temperature dependencies of the static D_{s} (△) fractal dimensions and the product $3v$ (•). At the percolation threshold temperature ($T_{\mathrm{p}} = 26.5$ °C) $D_{\mathrm{s}} = 3v$.

Another interesting feature of this approach is the possibility to interpret percolation in microemulsions in terms of the conventional distribution of relaxation times, $g(\tau)$. Using relationships (2.3), (2.5) and (2.6) we can present $g(\tau)$ as follows:

$$g(\tau) = C_g \left(\frac{\tau}{\tau_1}\right)^{(1-\eta-\Omega)/\eta} \exp\left[-\left(\frac{\tau}{\tau_m}\right)^{1/\eta}\right], \quad \tau_1 \leqslant \tau \leqslant \infty. \tag{2.11}$$

Here the normalization constant C_g may be calculated with taking into account the normalization condition $\int_{\tau_1}^{\infty} g(\tau)\,\mathrm{d}\tau = 1$:

$$C_g = \left(\eta \tau_m \cdot \left(\frac{\tau_m}{\tau_1}\right)^{(1-\Omega-\eta)/\eta} \Gamma\left[\Omega+1, \left(\frac{\tau_m}{\tau_1}\right)^{-1/\eta}\right]\right)^{-1}, \tag{2.12}$$

where

$$\Gamma(q,x) = \int_x^{\infty} y^{q-1} \exp(-y)\,\mathrm{d}y$$

is an incomplete Gamma-function.

Fig. 8 shows the relaxation time distribution $\tilde{g}(\tau) = g(\tau)/g_{\max}$ for two typical temperature values in the percolation onset region ($T_{\mathrm{on}} = 14$ °C) and the percolation threshold ($T_{\mathrm{p}} = 26.5$ °C). In this figure we plot the distribution function

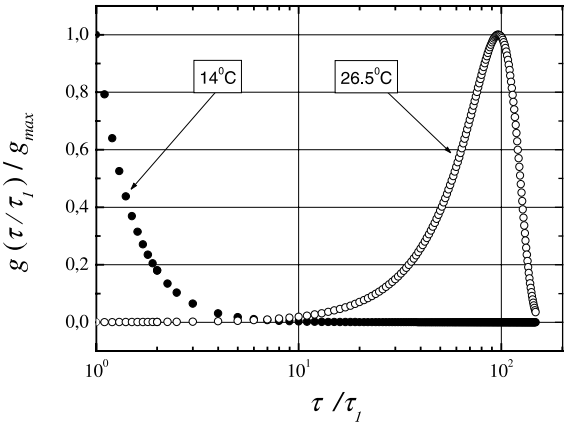

Fig. 8. The distribution functions $\tilde{g}(\tau) = g(\tau)/g_{\max}$ for two typical temperatures: at the percolation onset $T_{\mathrm{on}} = 14$ °C (•) and at the percolation threshold $T_{\mathrm{p}} = 26.5$ °C (○). Each distribution function is normalized on its maximal value $g_{\max}$ at the interval $1 \leqslant \tau/\tau_1 < \infty$.

normalized on its maximal value g_{max} at the interval $1 \leqslant \tau/\tau_1 < \infty$. The structural parameters η and Ω in (2.11) and (2.12) are calculated in this temperature interval by using the values of the fitting parameters μ, ν and relationship (2.8). The qualitative change of $\tilde{g}(\tau)$ is observed when the microemulsion approaches the percolation threshold. The power law of the distribution function at percolation onset testifies that the macroscopic *DCF* is the result of the small clusters averaging with a moderate value of polydispersity. Thus, near the percolation onset the relaxation occurs due to the grown of a significant number of parallel small clusters. Near the percolation, the function $\tilde{g}(\tau)$ is governed by the unimodal function with a well-distinguished maximum [11]. Such behavior is typical for the statistical contribution to the macroscopic *DCF* on the scale of the percolation cluster.

3. Dielectric relaxation of water absorbed in porous glasses

Non-Debye dielectric relaxation in porous silica glasses is another example of the dynamic properties of complex systems on a mesoscale. The porous silica glasses obtained from sodium borosilicate glasses are defined as bicontinuous random structures of two interpenetrating percolating phases, the solid and the pore networks. The pores in the glasses are connected to each other and the pore size distribution is narrow. The characteristic pore spacing depends on the method of preparation, and can be between 2 and 500 nm [59]. A rigid SiO_2 matrix represents the irregular structure of porous glasses. Water can be easily adsorbed on the surface of this matrix. The dielectric response is found to be very sensitive to the geometrical nano- and mesostructural features of the porous media and amount water molecules in the adsorptive layer on the pore surface.

The dielectric relaxation properties of silica glasses over broad frequency and temperature ranges have been investigated recently [60–63]. The typical spectra of the dielectric permittivity and losses associated with the relaxation of water molecules of the adsorptive layer for the studied porous glasses versus frequency and temperature are displayed in Figs. 9(a) and (b). One can see that the complex dielectric behavior can be described in terms of the four distributed relaxation processes.

The first relaxation process, which is observed in the low temperature region from −100 to +10 °C is due to the reorientation of the water molecules in ice-like water cluster structures. It was shown that the hindered dynamics of the water molecules located within the pores reflect the interaction of the absorptive layer with the inner surfaces of the porous matrix [60,62].

The second relaxation process has a specific saddle-like shape and is well marked in the temperature range of −50 to +150 °C. This relaxation process is thought to be a kinetic transition due to water molecule reorientation in the vicinity of a defect [62,63].

The third relaxation process is located in the low-frequency region and the temperature interval 50–100 °C. The amplitude of this process essentially decreases when the frequency increases and the maximum of the dielectric permittivity versus temperature has almost no temperature dependence (Fig. 10). Finally, the low-frequency ac-conductivity σ demonstrates an S-shape dependency with increasing temperature (Fig. 11), which is typical for percolation [43,61]. The dielectric relaxation process here is due to percolation of the apparent dipole moment excitation within the developed fractal structure of the connected pores [60,61,63]. This excitation is associated with the self-diffusion of the charge carriers in the porous net. Note that in the distinction from dynamic percolation in ionic microemulsions the percolation in porous glasses appears via the transport of the excitation through the geometrical static fractal structure of the porous medium.

In the high temperature region, above 150 °C, the glasses become electrically conductive and show an increase in dielectric permittivity and dielectric losses in the low-frequency limit. This relaxation process thought to be related to the Maxwell–Wagner–Sillars polarization process because of free charge carriers trapped at the interface, thus causing a build-up of macroscopic

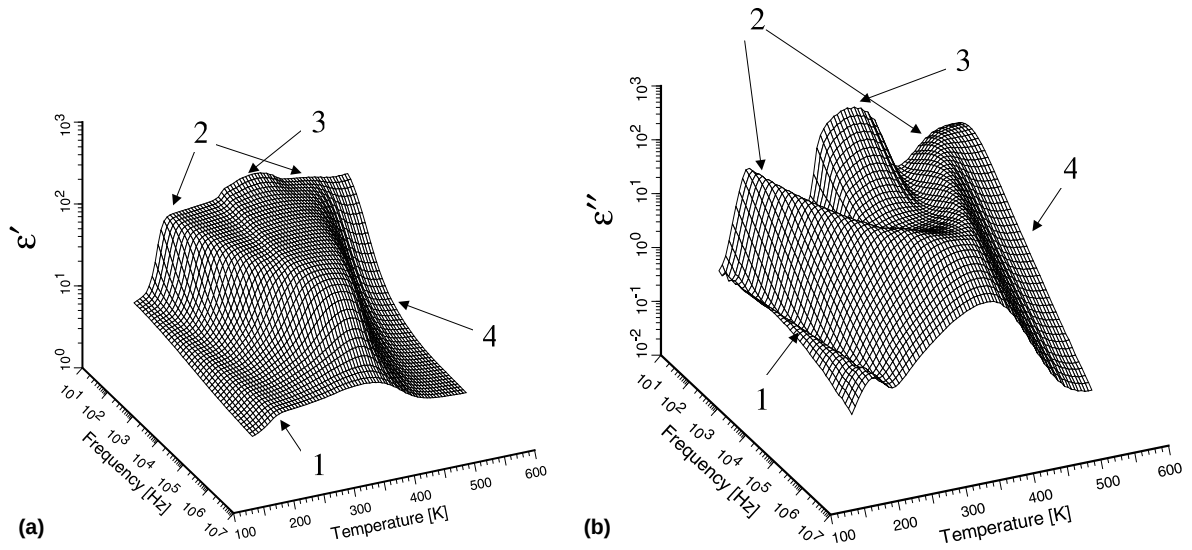

Fig. 9. The typical three-dimensional plot of the complex dielectric permittivity real ε' (a) and imaginary part ε'' (b) versus frequency and temperature for porous glass (sample E).

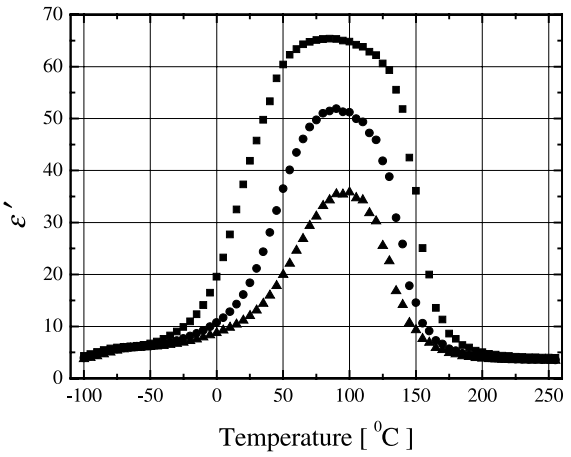

Fig. 10. The typical temperature dependence (for sample E) of the complex dielectric permittivity real part at different frequencies (■ – 8.65 kHz; ● – 32.4 kHz; ▲ – 71.4 kHz).

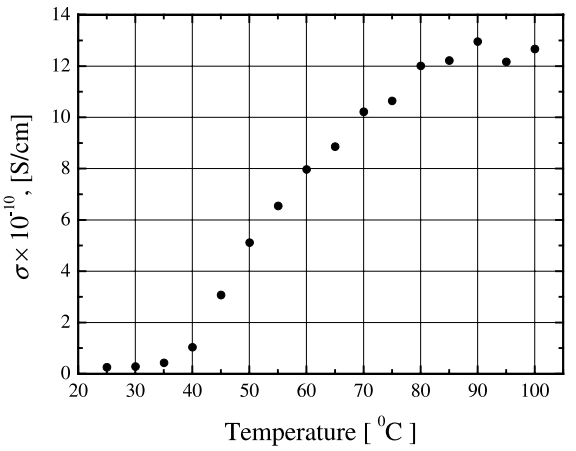

Fig. 11. Typical temperature dependence of the low-frequency ac-conductivity σ of the sample E.

charge separation, or space charge with a relatively long relaxation time [60].

In this section, we will consider in more detail the non-Debye dielectric response associated with percolation through the net of connected pore channels. The movement of charge carriers results in a transfer of the electric excitation within the channels along random paths. A detailed description of the relaxation mechanism associated with an excitation transfer based on regular and statistical fractal models is introduced in Section 2, where it was applied to the cooperative relaxation of ionic microemulsions at percolation. For both these models the time dependence behavior of the dipole correlation function $\Psi(t)$ may be written in the form of an asymptotic stretched-exponential term

$$\Psi(t) = \exp\left[-\left(\frac{t}{\tau_m}\right)^{D_p/3}\right]. \quad (3.1)$$

This result reflects the general ideas developed in [64,65] that transfer of the electric excitation in various condensed media occur by the transport from a donor unit to an acceptor unit through many parallel channels. In order to determine the value of the fractal dimension D_p of the paths of excitation transfer within the porous medium, the relaxation law (3.1) can be further fitted to the experimental correlation functions. If the fractal dimension of these paths coincides with the fractal dimension of the pore space, then it can be used for obtaining the porosity.

The dielectric relaxation at percolation is analyzed in time domain since the theoretical relaxation model described above is formulated for the dipole correlation function $\Psi(t)$. For this purpose the complex dielectric permittivity data were expressed in terms of the *DCF* using (1.3) and (1.11). Fig. 12 shows typical examples of the *DCF*, obtained from the frequency dependence of the complex permittivity at the percolation temperature, corresponding to several porous glasses studied recently [60–63].

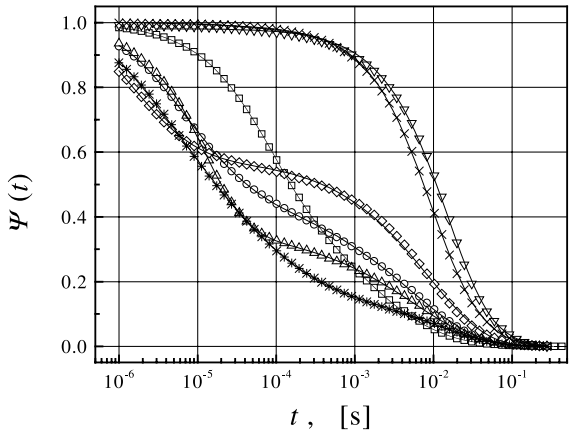

Fig. 12. Semi-log plot of the dipole correlation $\psi(t)$ of all the samples studied at the temperature corresponding to percolation (□ – sample A; ○ – sample B; △ – sample C; ▽ – sample D; ◇ – sample E; × – sample F; ∗ – sample G). The solid lines are the fitting curves of the sum of the *KWW* and the product of *KWW* and the power-law relaxation function.

As mentioned earlier, the *DCF* consists of two processes. Therefore, in order to separate the long-time percolation process, the *DCF* was fitted as a sum of two functions. The *KWW* function (3.1) was used for fitting the percolation process and the product (1.14) of the power law and the stretched exponential function (as a more common presentation of relaxation in time domain) was applied for the fitting of the additional short-time process. The values obtained for D_p of different porous glasses are presented in Table 1. The glasses studied are differing in the way of preparation, which affects the size of the pores, porosity and availability of second silica and ultra-porosity [60–63].

One can see that the fractal dimension of the excitation paths in sample A is close to unity. Topologically, this value of D_p corresponds to the propagation of the excitation along a linear path that may correspond to a presence of second silica within the pores. Indeed, the silica gel creates a subsidiary tiny scale matrix with an enlarged number of hydration centers within the pores. Since these centers are distributed in the pore volume, the excitation transmits through the volume and is not related to the hydration centers located on the pore surface of the connective pores. Due to the large number of hydration centers, and the short distance between the neighboring centers, the path can be approximated by a line with a fractal dimension close to unity.

The fractal dimensions of the excitation paths in samples B, C, and E have values between 1 and

Table 1
The values of *KWW* exponent v, fractal dimension D_p, porosity Φ_m obtained from relative mass decrement (A, B, C and D glasses) and gas adsorption (E, F and G glasses) measurements and average porosity $\langle\Phi_p\rangle$ estimated from dielectric spectra for porous glasses samples

Sample	v	D_p	Φ_m	$\langle\Phi_p\rangle$
A	0.33	0.99	0.38	0.33
B	0.63	1.89	0.48	0.47
C	0.44	1.31	0.38	0.37
D	0.83	2.50	0.50	0.68
E	0.65	1.96	0.27	0.49
F	0.80	2.40	0.43	0.63
G	0.73	2.20	0.26	0.56

2. In contrast, to sample A, the silica gel in these samples is leached out, i.e. water molecules are adsorbed on the inner pore surface. The values of D_p observed in samples B, C, and E can be explained in one of two ways. On one hand, the surface can be defractalized upon deposition of an adsorbed film of water, which results in the "smoothing" of the surface. On the other hand, the transfer of the excitation in these samples occurs along the inner pore surface from one hydration center to another. The distance between the centers is significantly larger than the small-scale details of the surface texture. Therefore, the fractal dimension observed is that of the chords connecting the hydration centers and should be less than 2, which is in agreement with the data obtained from the energy-transfer measurements [66,67].

The fractal dimensions of the excitation paths in samples D, F, and G are in the range between 2 and 3. Thus, percolation of the charge carriers (protons) is also moving through the SiO_2 matrix because of the availability of an ultra-small porous structure that occurs after special chemical and temperature treatment of the initial glasses [63].

Note that the fractal dimensions discussed here are the fractal dimensions of the excitation transfer paths connecting the hydration centers located on the inner surface of the pores. Due to the low humidity, all of the water molecules absorbed by the materials are bound to these centers. The paths of the excitation transfer span along the fractal pore surface and "depict" the backbone of clusters formed by the pores on a scale that is larger than the characteristic distance between the hydration centers on the pore surface. Thus, a fractal dimension of the paths D_p approximates the real surface fractal dimension in the considered scale interval. In this case, D_p can be also associated with the fractal dimension D_r of the porous space: $D_p \cong D_r$. Therefore, the fractal dimension D_p can be used for porosity calculations in the framework of the fractal models of the porosity.

The porosity Φ_p of a two-phase solid-pore system can be defined as the ratio of the mean volume of the whole empty space volume, V_p, to the whole volume, V, of a sample [68]:

$$\Phi_p = \frac{V_p}{V}. \tag{3.2}$$

Disordered porous media have been adequately described by the fractal concept [61,69]. It was shown that if the pore space is determined by its fractal structure, the *regular fractal* model could be applied [61]. This implies that for the volume element of linear size Λ, the volume of the pore space is given in units of the characteristic pore size λ by $V_p = G_g(\Lambda/\lambda)^{D_r}$, where D_r is the regular fractal dimension of the porous space, Λ coincides with the upper limit and λ with the lower limit of the self-similarity. The constant G_g is a geometric factor. Similarly, the volume of the whole sample is scaled as $V = G_g(\Lambda/\lambda)^d$, where d is the Euclidean dimension $(d = 3)$. Hence, the formula for the porosity in terms of the regular fractal model can be derived from Eq. (3.2), and is given by

$$\Phi_p = \left(\frac{\lambda}{\Lambda}\right)^{d-D_r}. \tag{3.3}$$

In general, in order to embrace variety of porous media the *random fractal* model can be considered [61,69]. Randomness can be introduced in the fractal model of a porous medium by the assumption that the ratio of the scale parameters λ/Λ is random in the interval $[\lambda/\Lambda, 1]$, but the fractal dimension in this interval is a determined constant. Hence, Eq. (3.3) reads as

$$\langle \Phi_p \rangle = \int_{\xi_0}^{1} \Phi_p(\xi, D_r) w(\xi)\, d\xi, \tag{3.4}$$

where ξ_0 is the minimal value of the scale parameter ξ in the interval $[\lambda/\Lambda, 1]$, and $w(\xi)$ measures the probability density to find some scale parameter in the range from ξ to $\xi + d\xi$.

For a percolating medium the generalized exponential pore-size distribution function of the scale for porous medium can be written as

$$w(\xi) \sim \xi^{\alpha_w} \exp(-a_w \xi^{b_w}). \tag{3.5}$$

This function accounts for the mesoscale region and comprises most of the listed distribution functions [61]. It includes three empirical parameters, α_w, β_w, and a_w. After ascertaining the relationships between these parameters and the properties of anomalous self-diffusion, fractal

morphology, and polydispersity of the finite pore-size, the physical significance can be assigned to these parameters in the framework of the percolation models [54].

On the length scale, larger than the pore sizes the morphology of the glass porous space can be modeled as a random-packed assembly of clusters formed by pores connected to each other [66,70]. In order to find the fractality in such porous glasses we must assume that the pore structure has a fractal character in a rather narrow scale range, i.e. the clusters are self-similar on the scale range less than two orders of magnitude in length ($\lambda/\Lambda \geqslant 0.01$). Hence, in the interval $[\lambda/\Lambda, 1]$ the uniform distribution function, $w(\xi) = w_0$, can be chosen as a first approximation of the function derived by Eq. (3.4). The value of w_0 is determined from the normalization condition $\int_{\xi_0}^{1} w(\xi)\,\mathrm{d}\xi = 1$, and reads as $w_0 = 1/(1-\xi_0)$. In this approximation, by substituting this uniform distribution function into integral (3.4) and integrating it, we obtain the relationship for the average porosity as

$$\langle \Phi_p \rangle = \frac{1}{1+d-D_r} \cdot \frac{1-\xi_0^{1+d-D_r}}{1-\xi_0}. \tag{3.6}$$

Then, by taking into account that $0.01 \leqslant \xi_0 \ll 1$ and $d = 3$, we obtain a simple approximate relationship between the average porosity of a glass and the fractal dimension of the pore space, which reads

$$\langle \Phi_p \rangle \approx \frac{1}{4-D_r}. \tag{3.7}$$

Note, that in our approximation, due to the randomized character of the fractal medium, the average porosity of the disordered porous glasses determined by Eq. (3.7) depends only on the fractal dimension D_r. The magnitude of the fractal dimension in Eq. (3.7) depends on the length scale of a measurement extending from λ to over Λ, where the minimal scale λ and the maximal scale Λ are determined by the measurement technique.

The results of the porosity calculation using Eq. (3.7) together with the fractal dimension determined from dielectric measurements are shown in the last column of Table 1. These values can be compared with the porosity Φ_m determined from the relative mass decrement (A, B, C and D glasses) and gas adsorption (E, F and G glasses) measurements shown in the same Table 1. Note that the values obtained from dielectric spectroscopy coincide with the porosity data obtained from the relative mass decrement method only for samples A, B and C. The porosity values for the other samples obtained through the dielectric measurements are significantly larger. This correlates with the availability of ultra-small porous structures with penetrability for the smallest charge carriers (such as protons) [63]. Thus, in the case of a net of super small open pores, the dielectric response is more sensitive and accurate in the determination of real porosity than any other conventional method.

4. Dielectric relaxation in porous silicon

The non-Debye dielectric relaxation was also observed also in porous silicon (*PS*) [22,71]. *PS* has attracted much attention recently, mainly due to the interesting optical and electro-optical properties of *PS* structures that can be utilized for device applications [72–75]. So far, most of the activity in this field has focused on the intense visible photoluminescence (*PL*) from *PS* and the underlying physical mechanism that is responsible for the generation of light. In addition, transport and dielectric relaxation phenomena in *PS* have also attracted considerable attention for injection type *PS* devices. It was mentioned in the previous section that the correlation between the morphology of porous media and their dielectric properties have already been studied in works [60,68]. In many porous media, these phenomena are directly related to the fractality, and the nano- and the mesostructural properties of these disordered systems [60,61,76–78]. In principle, one would expect to find a similar correlation between the microgeometry and the dielectric properties of *PS* media. However, several experimental reports indicate that such a simple picture cannot be applied to *PS*. For example, dc-conductivity measurements demonstrate the dual transport mechanism that has been assigned to thermally activated hopping and exited charged carriers tunneling [79]. As a result, carriers excited to the band tail would give rise to a

thermally activated dc-conduction with an activation energy of about 0.5 eV [22,80]. This activation energy is less than half the optical band-gap of *PS* deduced from *PL* experiments [72]. The ac-conductivity measurements in *PS* revealed complex transport properties due to a random walk in fractal geometry and thermally activated hopping, as in the case of dc conductivity [22]. Therefore, it is commonly accepted that both the nanogeometry, the nature of the Si nanocrystallites that form the *PS* medium and their surfaces as well as the host matrix all contribute to the electrical and optical properties of *PS*.

The dielectric relaxation properties in *PS* with different thicknesses have been investigated recently in the broad frequency and temperature region [71]. The dielectric properties of the *PS* samples were measured in the 20 Hz to 1 MHz frequency range and in the 173–493 K temperature interval. For all the dielectric measurements, the amplitude of a sinusoidal ac voltage source was kept constant at 1 V so that the average electric field across our sample is about 300 V/cm. It was verified that the response is linear with respect to the ac voltage amplitude such that a linear response analysis can be utilized for our sample.

Three-dimensional plots of both the measured real part ε' and the imaginary part ε'' of the complex dielectric permittivity versus frequency and temperature for 20 μm *PS* sample are shown in Figs. 13(a) and (b). From the figure one can identify three distinct processes, marked by I, II and III, defined as follows:

Low temperature process I. This process extends over low temperatures (170–270 K). Despite the fact that both the real and imaginary parts of the dielectric function display this process, it can be appreciated most by looking at ε'' at high frequencies and low temperatures where the local maximum, which shifted to higher frequencies with increasing temperature, can be easily detected.

Mid temperature process II. This process extends over the mid-range temperatures (300–400 K) and over low to moderate frequencies (up to 10^5 Hz).

High temperature process III. This process is very significant at high temperatures (>400 K). Its amplitude increases very rapidly with decreasing frequency for both the real and imaginary parts of the dielectric function. Similar processes were also observed for the 30 μm thickness sample.

All three processes exhibit a complex non-exponential relaxation behavior, and correspond to another good example of the non-Debye dielectric response. Let us consider here in more detail only the low and middle temperature processes.

4.1. Low temperature process I

Typical spectra of the real and the imaginary parts of the dielectric permittivity at 233 K for the 30 μm sample are shown in Fig. 14. Excellent fits for both the real and the imaginary parts of the dielectric permittivity for all temperatures (170–270 K) were obtained by taking into account two *HN* (Eq. (1.10)) processes and the Jonscher term. Two relaxation times (τ_1 and τ_2) are extracted from the fitting of the *HN* processes for both samples and are plotted versus inverse temperature in Fig. 15. Both relaxation times demonstrate Arrhenius behavior, $\tau_j \propto \exp(-E_{a,j}/kT)$, with $E_{a,j}$ being the activation energy of the process. The fitting (shown by the solid lines in Fig. 15, the first and the second relaxation processes) yields activation energies of 0.28 and 0.4 eV for the 20 μm sample and of 0.2 and 0.3 eV for the 30 μm sample, respectively. Note that for all temperatures and samples used in this study $\beta = 1$. Hence, the *CC* relaxation type is adequate for a description of the low-temperature relaxation processes in *PS*.

A model was proposed to explain the existence of two activation energies corresponding to two groups of excited states in *PS* [71], based on the presentation of *PS* as a random network of Si nanocrystallites [73,80]. Hence, these excited states would contribute to thermally activated transport processes with temperature dependent relaxation times as observed in our measurements and shown in Fig. 15.

4.2. Mid temperature process II and porosity determination

In the previous work [81], we used a superposition of two Jonscher terms of the form

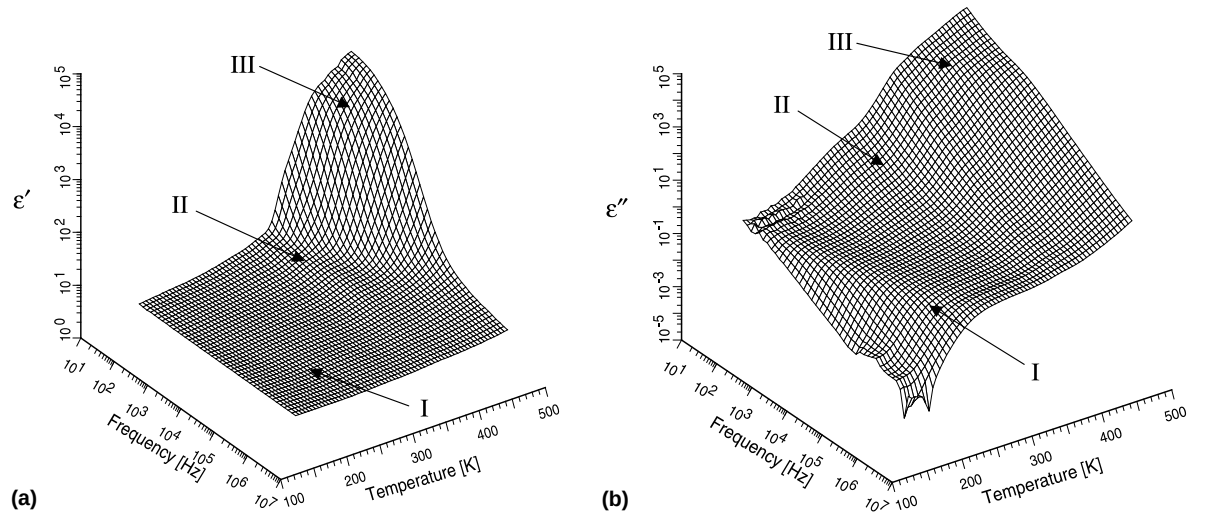

Fig. 13. Three-dimensional plots of the frequency and temperature dependence of the real ε' (a) and imaginary part ε'' (b) of the complex dielectric permittivity for the 20 μm *PS* sample.

$B_1(i\omega)^{u_1-1} + B_2(i\omega)^{u_2-1}$ to describe mid-temperature relaxation processes. The results of our fitting were in good agreement with those of Ben-Chorin et al. [22]. They were discussed in terms of the transport of charged carriers at the different scales. The high-frequency Jonscher exponent was associated with the typical size of the Si nanocrystallites, while the low-frequency (*LF*) exponent was assigned to the transport of charged carriers across a disordered fractal structure of porous silicon [81–83]. At the same time the mid temperature process II demonstrates several specific features that are similar to those observed in other porous systems that were discussed in the previous section [60–63]. The amplitude of this process essentially decreases when the frequency increases (Fig. 13(a)). Further more, the maximum of the dielectric permittivity versus temperature has almost no temperature dependence (Fig. 13). Finally, the low-frequency ac conductivity increases with the increase in temperature and has an S-shape dependency (Fig. 16), which is typical for percolation processes [43,61]. Thus, we will analyze this process in the same way we did for percolation in porous glasses (see Section 3) [60,61,76–78].

The experimental macroscopic *DCF* for *PS* samples with porous layers of 20 and 30 μm, obtained by inverse Fourier transform, are shown in Fig. 17. The correlation functions then were fitted by *KWW* expression (1.12) with determination of the fractal dimension D_p of the percolation path. Applying the same routine to determine the porosity in other porous systems [61,76–78], the average porosity of the porous silicon was evaluated with the help of relationship (3.7). The results are presented in Table 2. The values of porosity determined from the dipole correlation function analysis are in good agreement with porosity values determined by weight loss measurements during *PS* preparation (before and after the anodization process).

Thus, the non-Debye dielectric behavior in *AOT* microemulsions, silica glasses, and *PS* has similar properties. These systems exhibit an intermediate temperature percolation process that is associated with the transfer of the electric excitations through the random structures of fractal paths. It was shown that at the mesoscale range the fractal dimension of the complex material morphology (D_r for porous glasses and D_s for the microemulsions) coincides with the fractal dimension D_p of the path structure. This value can be evaluated by the fitting of the experimental *DCF* to the stretched-exponential relaxation law (3.1).

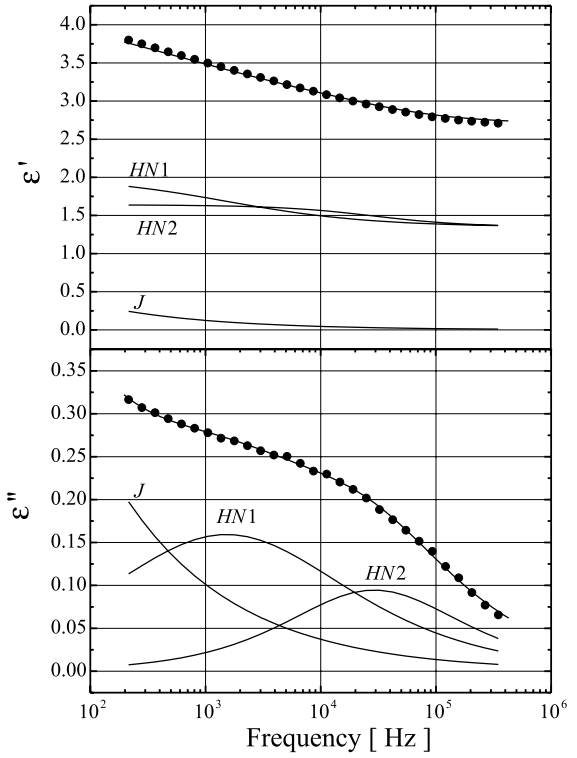

Fig. 14. The measured real (top) and imaginary (bottom) parts of the complex dielectric permittivity versus frequency at low temperature (233 K). The dashed lines marked *J*, *HN* 1 and *HN* 2 are the Jonscher term (1.13) and the two *HN* (1.12) semi-empirical terms, respectively, used for fitting of the experimental data points (●). The solid lines are superpositions of the above terms, which fit the experimental data. The sample thickness is 30 μm.

5. Symmetric dielectric spectrum broadening in disordered materials

In the previous sections, we presented several examples of the non-exponential dielectric response in time domain. These have all obeyed the two models developed in Section 2. These models enable us to determine some topological properties of the investigated complex systems. However, the frequency representation has its own advantages. In particular, the non-dissipative part of the system response to an external perturbation and the dissipative part are clearly separated in frequency domain as the real and imaginary parts of the complex permittivity, while in time domain these

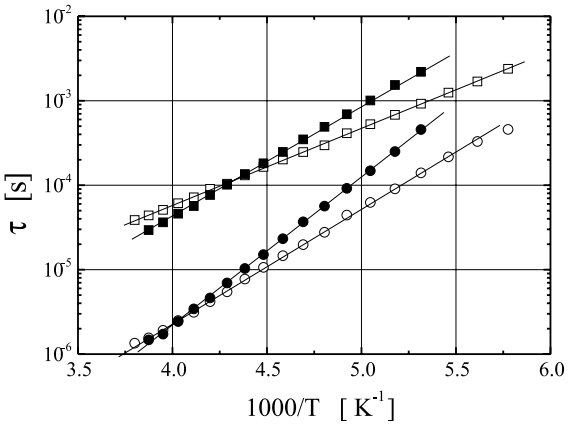

Fig. 15. Arrhenius plot (semi-log scale versus the inverse temperature) of the two characteristic relaxation times, τ_1 (■) and τ_2 (●) for the 20 μm sample, and τ_1 (□) and τ_2 (○) for the 30 μm sample, for low temperature process I.

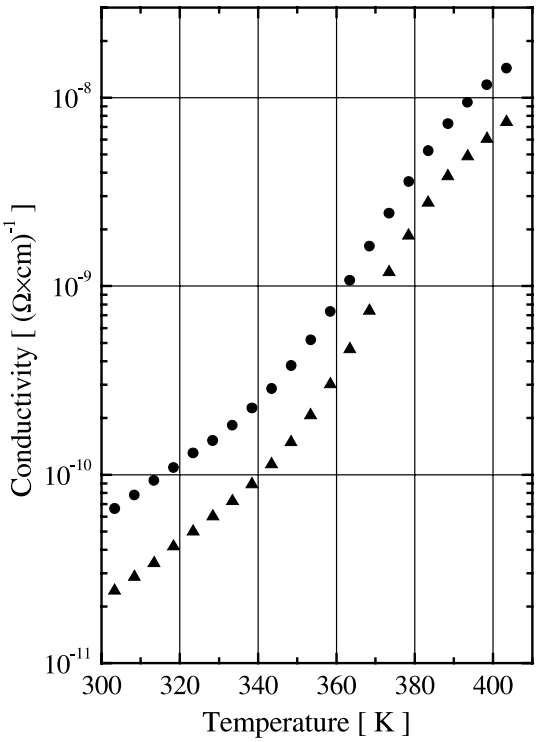

Fig. 16. Temperature dependence of the low-frequency conductivity of the 20 μm sample (●), and the 30 μm sample (▲).

effects are "mixed" together in the relaxation function. The separation of response itself and dissipative effects in time domain is not obvious,

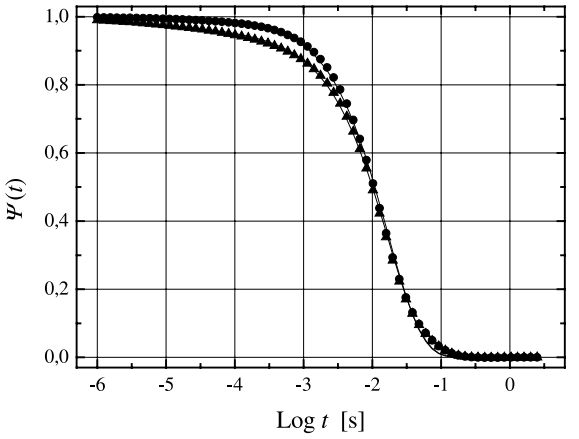

Fig. 17. Semi-log plot of the macroscopic correlation function of the 20 μm sample (●) and the 30 μm sample (▲) at the temperature corresponding to percolation. The solid lines correspond to the fitting of the experimental data by *KWW* relaxation function.

Table 2
The values of *KWW* exponent v, fractal dimension D_p, porosity Φ_m obtained from relative mass decrement measurements and average porosity $\langle\Phi_p\rangle$ estimated from dielectric spectra for porous silicon samples of 20 and 30 μm thickness [71]

Sample thickness	v	D_p	Φ_m	$\langle\Phi_p\rangle$
20 μm	0.88	2.64	0.78	0.74
30 μm	0.87	2.61	0.75	0.72

although it is possible in principle by using the appropriate integral transform. In spite of the existence of the one mapping between the time and frequency domain by the Laplace transform, the separation in frequency representation may at times be more convenient for analysis of the dynamic processes in complex systems.

5.1. Relaxation peak broadening and its relationship to the dynamical and topological properties

As mentioned in the introduction, the experimental dielectric response in frequency domain for most complex systems cannot be described by a simple Debye expression (1.6) with a single dielectric relaxation time. In most general way this dielectric behavior can be described by the phenomenological *HN* formula (1.10).

Usually the exponents α and β are referred to as measures of symmetrical and unsymmetrical relaxation peak broadening. These names are the consequence of the fact that the imaginary part of the complex permittivity for the *HN* dielectric permittivity shows power-law asymptotic forms $\mathrm{Im}\{\varepsilon^*(\omega)\} \sim \omega^{\alpha}$ and $\mathrm{Im}\{\varepsilon^*(\omega)\} \sim \omega^{-\alpha\beta}$ in the low- and high-frequency limits, respectively. The experimental data show that α and β are strictly dependent on temperature, structure, composition, pressure and other controlled physical parameters [2,15,16,84–91]. There is no complete understanding or universal models of these dependencies for the time being. However, over the last years significant progress in this direction has been made [19,20,27–29,92–98]. Many efforts [99–101] were undertaken in order to understand the relaxation dynamics of the glass-forming liquids and different polymer mixtures before the work [102] where the concentration fluctuation model was introduced. In the framework of this model, a reasonable explanation of the α-relaxation process in homogeneous polymer mixtures was presented. Although the relaxation peak broadening was discussed in [102] there are no relationships derived for exponents α and β versus structural or dynamical parameters.

This kind of non-exponential response is observed in numerous physical systems and does not only describe their dielectric properties. For instance, in the works [95,96] the Monte Carlo simulation of random walks on two-dimensional fractal structures was carried out. It was shown there that the complex susceptibility of this process has the power-law frequency asymptotic similar to the *HN* type. Moreover, the model coupling theory [87] ascribes to the power-law exponents a universal nature by virtue of the universality of the correlation functions for different dynamical variables.

There is also a set of works where the mathematical formalism of fractional calculus [103,104] was applied to the anomalous diffusion and relaxation problems. The physical applications as well as the mathematical issues of fractional calculus were recently investigated in the book [93]. The review [27] discusses anomalous diffusion in detail. In the works [19,20,92], the relaxation

equation for the *HN* processes was obtained. Nevertheless, for the time being there is no unambiguous clear understanding of the non-exponential response in complex disordered heterogeneous systems. Therefore, an understanding of the relationship between α and β exponents and the physical properties of the systems is very important.

In this section we will consider the specific case of the *HN* formula $\beta = 1$, $0 < \alpha < 1$, corresponding to symmetric relaxation peak broadening or to the so-called *CC* law [13]. The complex dielectric permittivity $\varepsilon^*(\omega)$ for the *CC* process is represented in the frequency domain as

$$\varepsilon^*(\mathrm{i}\omega) = \varepsilon_\infty + \frac{\varepsilon_s - \varepsilon_\infty}{1 + (i\omega\tau)^\alpha}. \tag{5.1}$$

In order to explain the non-Debye response (5.1) it is possible to use the memory function approach [19,20,27,92,105–107]. Thus, the normalized dipole correlation function $\Psi(t)$ corresponding to a non-exponential dielectric relaxation process obeys the equation

$$\frac{\mathrm{d}\Psi(t)}{\mathrm{d}t} = -\int_0^t m(t-t')\Psi(t')\,\mathrm{d}t', \tag{5.2}$$

where $m(t)$ is the memory function, and t is the time variable. The specific form of the memory function is dependent on the features of relaxation.

After Laplace transform (1.4), in virtue of the convolution form, Eq. (5.2) reads as

$$pF(p) - 1 = -M(p)F(p), \tag{5.3}$$

where $F(p)$ and $M(p)$ are Laplace images of $\Psi(t)$ and $m(t)$. Combining (5.3) with (5.1) and taking into account the relationship between the complex permittivity and the correlation function, (1.3), one can obtain the Laplace image of the memory function for the *CC* process in the form

$$M(p) = p^{1-\alpha}\tau^{-\alpha}. \tag{5.4}$$

Since $0 < \alpha < 1$ the exponent in Eq. (5.4) $1 - \alpha > 0$. The mathematical implication is that $M(p)$ (5.4) is a multi-sheet function of complex variable p. In order to represent this function in the time domain one should to select the schlicht domain using supplementary physical reasons [108]. These computational constraints can be avoided by using Riemann–Liouville fractional differential operator ${}_0D_t^{1-\alpha}$. By definition [103,104] of the Riemann–Liouville fractional differentiation operator

$${}_0D_t^{\gamma}[h(t)] = \frac{\mathrm{d}}{\mathrm{d}t}{}_0D_t^{\gamma-1}[h(t)], \quad 0 < \gamma \leqslant 1, \tag{5.5}$$

where

$${}_0D_t^{-v}[g(t)] = \frac{1}{\Gamma(v)}\int_0^t (t-t')^{v-1}g(t')\,\mathrm{d}t', \quad 0 < v \leqslant 1, \tag{5.6}$$

is the Riemann–Liouville fractional integration operator. In this last formula $\Gamma(v) = \Gamma(v,0)$ is the complete Gamma-function. Thus, from the definitions one can easily see that the Laplace image of ${}_0D_t^{1-\alpha}[\Psi(t)]$ is

$$\hat{L}[{}_0D_t^{1-\alpha}[\Psi(t)]] = p^{1-\alpha}F(p) - C, \quad \text{where} \quad C = D_t^{-\alpha}[\Psi(t)]|_{t=+0}. \tag{5.7}$$

Taking (5.7) into account we can rewrite Eq. (5.2) with the memory function (5.4) as follows:

$$\frac{\mathrm{d}\Psi(t)}{\mathrm{d}t} = -\tau^{-\alpha}{}_0D_t^{1-\alpha}[\Psi(t)]. \tag{5.8}$$

Note that the relationship between the complex permittivity and correlation function (1.3), together with Eq. (5.1) leads directly to the requirement that $C = 0$.

Eq. (5.8) was already discussed elsewhere [19,20,92,109] as a phenomenological representation of the dynamic equation for the *CC* law. Thus, Eq. (5.8) shows that since the fractional differentiation and integration operators have a convolution form it can be regarded as consequence of the memory effect. A comprehensive discussion of the memory function (5.4) properties is presented in [19,20,92]. Accordingly, Eq. (5.8) holds for some cooperative domain and describes the relaxation of an ensemble of microscopic units. Each unit has its own microscopic memory function $m_\delta(t)$, which describes the interaction between this unit and the surroundings (interaction with the statistical reservoir). The main idea of such an interaction was introduced in [19,20,92] and suggests that $m_\delta(t) \sim \sum_i \delta(t_i - t)$ (see Fig. 18). It

reflects the interrupted interaction between the relaxing unit and its neighbors. The time moments t_i (the time position of the delta functions) are the moments of the interaction. The sequence of t_i, constructs a fractal set (the Cantor set for example) with a fractal dimension $0 < d_f \leqslant 1$. This statement is related to the idea that cooperative behavior provides some ordering and long lasting scaling. Following these assumptions the memory function $m(t)$ for a cooperative domain can be obtained as a result of averaging over the ensemble of $m_\delta(t)$ (see Fig. 19 where for more convenient representation $I(t) = \int_0^t m(t')\,dt'$ is plotted instead of $m(t)$. The requirements of measure conservation in the interval $[0, 1/\zeta]$ and conservation of the fractal dimension d_f for all $m_\delta(t)$ give this averaging as [19,92]

$$m(t) = \int_{-1/2}^{1/2} m_\delta(\zeta^{-u}t)\zeta^{-u(1-d_f)}\,du \tag{5.9}$$

and

$$M(p) \sim p^{1-d_f}.$$

Thus, the memory function (5.4) is a cooperative one and the *CC* behavior appears on the macroscopic level after averaging over the ensemble of microscopic dipole active units. Comparing (5.4) and (5.9) one can establish that $\alpha = d_f$. This result once again highlights the fact that in this model the fractal properties on a microscopic level induce the power-law behavior of memory functions (5.4), (5.9) and *CC* permittivity (5.1) on a macroscopic level.

By definition [55,56], the fractional dimension is given by

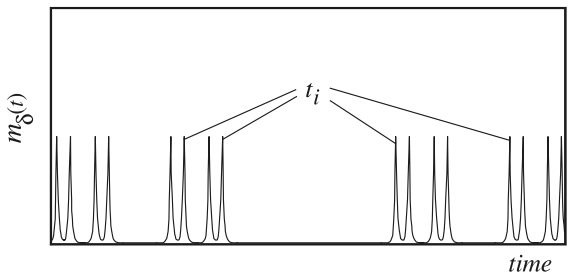

Fig. 18. Schematic picture of $m_\delta(t)$ dependency. t_i are the time moments of the interaction that construct in time a fractal Cantor set with dimension $d_f = \ln 2/\ln 3 \cong 0.63$.

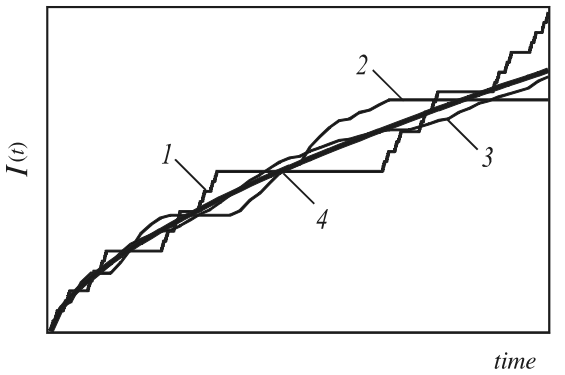

Fig. 19. Schematic presentation which illustrates averaging of $m(t)$ over an ensemble of microscopic units. Here $I(t) = \int_0^t m(t')\,dt'$. Curve 1 corresponds to the cooperative ensemble of a single microscopic unit with t_i distributed by the Cantor set. Curve 2 represents the ensemble of three units of the same type, Curve 3 – 10 units. Curve 4 corresponds to 1000 units in ensemble. The latter exhibits the power-law behavior $I(t) \sim t^{\ln 2/\ln 3}$.

$$d_f = \alpha = \frac{\ln(N)}{\ln(\zeta)}. \tag{5.10}$$

Here the scaling parameter ζ is the dimensionless time interval size and N is the number of delta functions (relaxation acts) in that interval. However, a characteristic time constant of the *CC* process is the relaxation time τ. Thereby, the scaling parameter ζ and the relaxation time should be proportional to each other

$$\zeta = \frac{\tau}{\tau_0}. \tag{5.11}$$

The constant minimal τ_0 is the cutoff time of the scaling in time.

In the general case, different physical conditions can determine the fractal properties of the microscopic memory function $m_\delta(t)$ and, consequently, the power-law time dependence of the macroscopic memory function (5.9). However, there is a computer simulation proof [95] that an anomalous relaxation on a fractal structure exhibits a *CC* behavior. Therefore, one can suppose that the memory function (5.9) has its origin in the geometrical self-similarity of the investigated system. Thus, the scaling parameter N actually is the number of points where the relaxing units are interacting with the statistical reservoir (i.e. by the

ergodic assumption – the number of relaxation acts on a microscopic level for a cooperative domain). The assumption of geometrical self-similarity of the considered system suggests that this number is

$$N = G\left(\frac{R}{R_0}\right)^{d_G}. \tag{5.12}$$

Here, d_G is a spatial fractal dimension of the point set where relaxing units are interacting with the surroundings. R is the size of a sample volume section where movement of one relaxing unit occurs. R_0 is the cutoff size of the scaling in the space or the size of the cooperative domain. G is a geometrical coefficient about unity, which depends on the shape of the system heterogeneity. For example, the well-known two-dimensional recurrent fractal Sierpinski carpet has $d_G = \ln(8)/\ln(3) \approx 1.89$, $G = \sqrt{3}/4 \approx 0.43$ [55].

The relaxation process can be accompanied by a diffusion act. Thereby, the mean relaxation time for such kinds of disordered systems is the time during which the relaxing microscopic structural unit would move a distance R. The Einstein–Smoluchowski theory [110,111] gives the relationship between τ and R as

$$R^2 = 2d_E D\tau, \tag{5.13}$$

where D is the diffusion coefficient and d_E is the Euclidean dimension. Thus, combining the relationships (5.10)–(5.13) one can get the relationship between the exponent α and the mean relaxation time in the form

$$\alpha = \frac{d_G}{2}\frac{\ln(\tau\omega_s)}{\ln(\tau/\tau_0)}, \tag{5.14}$$

where $\omega_s = 2d_E G^{2/d_G} D/R_0^2$ is the characteristic frequency of the diffusion process. This equation establishes the relationship between the *CC* exponent α, the relaxation time τ, the geometrical properties (fractal dimension d_G), and the diffusion coefficient (through ω_s).

5.2. Polymer–water mixtures

The first mention of the $\alpha(\tau)$ dependencies was in the experimental work [89]. The dielectric relaxation data of the water in the mixtures with seven water-soluble polymers were presented there. It was found that in all these solutions relaxation of water obeys the *CC* law, while the bulk water exhibits the well-known Debye-like pattern [112,113]. Another observation was that α is dependent not only on the concentration of solute but also on the hydrophilic (or hydrophobic) properties of the polymer. The seven polymers are: poly(vinylpyrrolidone) (*PVP*; weight average molecular weight (Mw) = 10,000), poly(ethylene glycol) (*PEG*; Mw = 8000), poly(ethylene imine) (*PEI*; Mw = 500,000), poly(acrylic acid) (*PAA*; Mw = 5000), poly(vinyl methyl ether) (*PVME*; Mw = 90,000), poly(allylamine) (*PAlA*; Mw = 10,000), and poly(vinyl alcohol) (*PVA*; Mw = 77,000). These polymers were mixed with different ratios (up to 50% of polymer in solution) to water and measured at a constant room temperature (25 °C) [89].

Here we would like to sketch a recent application [114] of model (5.14) to these systems. In Fig. 20 the experimental dependencies of *CC* exponent α versus τ together with the fitting curve are presented. The values of the fitting parameters are in Table 3.

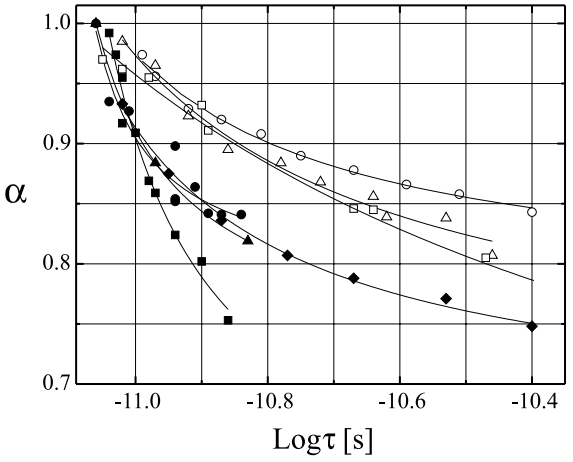

Fig. 20. *CC* exponent α versus relaxation time τ for *PVA* (●), *PAlA* (▲), *PAA* (■), *PEI* (◆), *PEG* (○), *PVME* (△) and *PVP* (□) samples. The curves correspond to the model described in Section 5. The full symbols correspond to the hydrophilic polymers and the open symbols correspond to the hydrophobic samples.

Table 3
The space fractional dimension d_G, the cutoff time of the scaling in the time domain τ_0, the characteristic frequency ω_s and estimated self-diffusion coefficient for the polymer water mixtures[a]

Sample	d_G	τ_0 (ps)	$\omega_s \times 10^{-11}$ (Hz)	$D \times 10^9$ (m^2 s^{-1})
PVA	1.56 ± 0.09	7.18 ± 0.74	1.47 ± 0.21	3.31
PAlA	1.43	6.46	1.74	3.92
PAA	1.12 ± 0.17	6.34 ± 0.83	2.08 ± 0.68	4.68
PEI	1.33 ± 0.02	4.89 ± 0.45	2.67 ± 0.40	6.01
PEG	1.54 ± 0.04	4.45 ± 0.74	2.78 ± 0.63	6.26
PVME	1.38 ± 0.10	3.58 ± 1.23	4.24 ± 2.47	9.54
PVP	1.00 ± 0.01	0.79 ± 0.11	127 ± 34	286

[a] For the sample *PAlA* there are only three experimental points. For this reason it is impossible to determine the mean square deviation value and consequently the confidence intervals for the fitting parameters.

It is well known [112,113] that the macroscopic dielectric relaxation time of the bulk water (8.27 ps at 25 °C) is about 10 times greater than the microscopic relaxation time of a single water molecule, which is about one hydrogen bond lifetime [115–118] (about 0.7 ps). This fact follows from the bulk water associative structure when the macroscopic relaxation time reflects the cooperative relaxation process in some cluster of water molecules.

In the framework of the model presented above the microscopic relaxation time of water molecule is equal to the cutoff time of the scaling in time domain τ_0. For the most hydrophilic polymer, *PVA*, the strong interaction between the polymer and the water molecule results in the greatest value of microscopic relaxation time τ_0, only 10% less than the macroscopic relaxation time of the bulk water. The most hydrophobic polymer, *PVP*, has the smallest value of a single water molecule microscopic relaxation time, which is almost equal to the microscopic relaxation time of bulk water (see Table 3). Therefore, weakening the hydrophilic properties (or intensifying the hydrophobic properties) results in a decreasing of interaction between the water and the polymer and consequently in the decrease of τ_0.

The interaction between the water and the polymer occurs in the vicinity of the polymer chains and only the water molecules situated in this interface are affected by the interaction. The space fractal dimension d_G in this case is the dimension of the macromolecule chain. If a polymer chain is stretched as a line, then its dimension is 1. In any other conformation, the wrinkled polymer chain has a larger space fractal dimension, which falls into the interval $1 < d_G < 2$. Thus, it is possible to argue that the value of the fractal dimension is a measure of polymer chain meandering. Straighter (probably more rigid) polymer chains have d_G values close to 1. More wrinkled polymer (probably more flexible) chains have d_G values close to 2 (see Table 3).

The presence of a polymer in the water affects not only the relaxation but the diffusion of the solvent as well. For an estimation of the diffusion coefficient, we can use the following expression:

$$D \cong \frac{\omega_s R_0^2}{2d_E}, \tag{5.15}$$

which is directly derived from the definition of the characteristic frequency ω_s. It was assumed in this last expression that the geometrical factor $G = 1$. In our case the scaling cutoff size in space is equal to the diameter of a water molecule $R_0 \approx 3$ Å [119]. The Euclidean dimension of the space where diffusion occurs is the nearest integer number greater than the fractal dimension. Thus, $d_E = 2$. The results of this estimation are in Table 3. The diffusion coefficient for the bulk water [119] at 25 °C is 2.57×10^{-9} m^2 s^{-1}. The presence of a polymer in the water prevents clusterization of water and relieves the diffusion. However, the strong interaction between polymer and water for hydrophilic samples slows down the diffusion. The competition of these two effects leads to the clear tendency of the diffusion coefficient to increase with an increase of hydrophobicity (see Table 3).

Note that the polymer affects only water molecules situated in the vicinity of the polymer chains. Thus, the estimated diffusion coefficient corresponds only to these water molecules and is not dependent on the polymer concentration. The averaged self-diffusion coefficient estimated for the entire polymer–water mixture should be different depending on the polymer concentration.

5.3. Microcomposite material

Another example of an application of Eq. (5.14) is on microcomposite polymer material. We have performed dielectric measurements of the glass transition relaxation process in a nylon 6,6 quenched sample in amorphous (*QN*), crystalline nylon 6,6 sample (*CN*) and microcomposite sample (*MCN*), which is the same crystalline nylon 6,6 but with incorporated kevlar fibers [120].

The quantitative analysis of the dielectric spectra of the glass-transition process was carried out by fitting the isothermal dielectric loss data according to the *HN* law (1.10). It was found from the fitting that $\beta = 1$ for the glass-transition process in all of the samples. The glass-transition relaxation process in these systems is due to the motion of a polymer chain that is accompanied by a diffusion act. In general, the diffusion of a polymer chain is more complex than the Brownian model for diffusion [121,122]. However, in all the models the dependence of $\langle R^2 \rangle$ on time t is linear in the time scales associated with a monomeric link and in the time scale associated with the mobility of the entire chain. For this particular example, Eq. (5.13) describes the mobility of the polymer groups in the microscopic levels, i.e. at the scale of a monomeric link.

The experimental α versus τ dependencies for these samples, together with the fitting curves, are shown in Fig. 21. Note that in contrast to the previous example, these data are obtained at a constant sample composition. In this case, variations of parameters α and τ are induced by temperature variation. As mentioned above, the exponents α as well as the relaxation time τ, are the functions of different experimentally controlled parameters. The same parameters can affect the structure or the diffusion simultaneously. In particular, both α and τ are functions of temperature. Thus, the temperature dependence of the diffusion coefficient in (5.13) should be considered. Let us consider the temperature dependence of diffusion coefficient D,

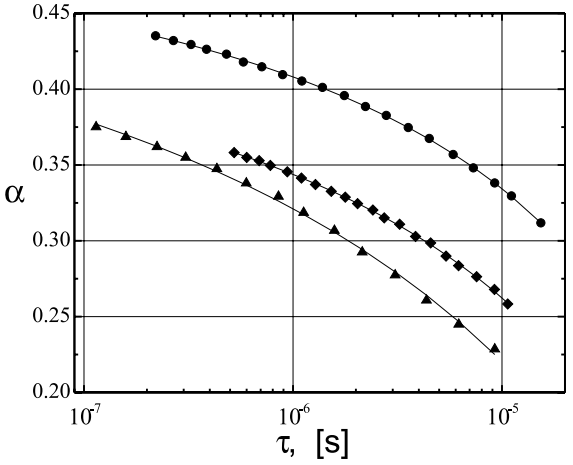

Fig. 21. The dependence of α versus relaxation time τ for *QN* (•), *CN* (▲) and *MCN* (◆) samples. The curves correspond to the model described in Section 5.

$$D = D_0 K(T), \tag{5.16}$$

where $K(T)$ is a dimensionless function that represents temperature dependence of the diffusion coefficient. D_0 is the appropriate constant with the dimension [$m^2\ s^{-1}$]. An increase of the diffusion coefficient with increasing temperature also signifies an increase of the characteristic spatial scale R_0 (cutoff size of the scaling in the space). Let us assume that R_0^2 is proportional to the diffusion coefficient D and obeys the Einstein Smoluchowski theory

$$R_0^2 = 2d_E D\tau_{max}, \tag{5.17}$$

where τ_{max} is the long-time limit of the scaling. Thus, combining together (5.16) and (5.17) with (5.11)–(5.13) we can obtain the relationship between the *CC* exponent α and relaxation time τ in a form similar to (5.14)

$$\alpha = \frac{d_G}{2}\frac{\ln(\tau\omega_0)}{\ln(\tau/\tau_0)} \tag{5.18}$$

with substitution of ω_s by $\omega_0 = G^{2/d_G}/\tau_{max}$. The latter relationship shows that under assumption

(5.17) the temperature dependence of the diffusion coefficient does not change the form of the α versus τ relationship.

The average length of a nylon 6,6 polymer chain is about 50–100 μm (each polymer chain contains about 10^5 groups while the length of a polymer group r_g is about 10 Å). This length is comparable to the thickness of a sample 120–140 μm [120]. Thus, the movement of the chains is most likely occurring in the plane of the sample. This fact correlates with the values of the space fractional dimension d_G. For all of the samples $d_G \in (1,2)$ (see Table 4). Thereby, the Euclidean dimension of the space in which chain movement occurs is $d_E = 2$.

Although there is no unambiguous data for the mesoscale structure of the samples under investigation at this time, nevertheless it is possible to estimate the order of magnitude of some physically significant quantities from the cutoff time τ_0 and characteristic frequency ω_0 values. Despite the fact that ω_0 and ω_s have different physical significance, for the estimation one can neglect temperature dependence of the diffusion coefficient and assume that $R_0^2 \approx 10^{-16}$ m^2 (R_0 is the cube root of the volume occupied by one polymer chain), $G \approx 1$. Then, the self-diffusion coefficient evaluated by expression (5.15) falls into the interval 10^{-14} to 10^{-13} m^2 s^{-1}, which is typical for such polymer materials [123–125].

The cutoff time τ_0 is related to the size of the cooperative domain l_c by $l_c^2 = 4D\tau_0$. Thus, in the two-dimensional case one can estimate the number of polymer groups n_g in the cooperative region as $n_g = l_c^2/r_g^2 \approx 10^2$, which is in fair agreement with the results obtained in the paper [126].

Table 4
The space fractional dimension d_G, the cutoff time of the scaling in the time domain τ_0 and the characteristic frequency ω_0 for polymer quenched (*QN*), crystalline (*CN*) and microcomposite samples (*MCN*)

Sample	d_G	τ_0 (ms)	ω_0 (kHz)
QN	1.12 ± 0.01	1.1 ± 0.1	5.9 ± 0.3
CN	1.20 ± 0.05	5.8 ± 4.4	9.7 ± 1.9
MCN	1.04 ± 0.02	1.5 ± 0.4	8.1 ± 0.7

One can also see from Table 4 that the presence of either the crystalline phase or the kevlar fibers in a sample leads to an increase of the cutoff time τ_0, indicating a slowdown of the relaxation process. Their presence also leads to an increase of the ω_0 value as well. This is a manifestation of a decreasing mobile polymer chain length.

6. Discussion

Generally speaking, through all the previous sections we tried to present several recent applications of two non-Debye dielectric relaxation models: the model relaxation induced by the percolation process (dynamic or static) and the model of *CC* relaxation. These models describe the properties of the phenomena discussed and provide some general information about the investigated disordered materials.

The electric percolation phenomena in different systems such as ionic microemulsions, porous silicon, and porous glasses can actually be analyzed in the framework of one universal approach based on the idea of charge carrier transport through the fractal network clusters. This model describes the growth of the fractal pre-percolation clusters.

The other model describes *CC* relaxation in polymer–water mixtures, microcomposite and polymer material. The main idea of this model is the interrupted fractal interaction between the microscopic units and the surroundings. These two models are quite general. It is shown above that each model is applicable to different systems with different charge carrier natures and different types of interactions with surroundings.

Nevertheless, each model is applicable only to one particular phenomenon and does not consider any basic ideas of "strange kinetic" behavior. Obviously, the "strange kinetic" is a very wide class of phenomena, which cannot be covered by the limited number of models, and has few specific features. Most famous among these characteristics is the power-law (or stretched exponent) asymptotic with a fractional exponent for the dipole correlation function in time domain or dielectric permittivity in frequency domain (see Eq. (1.10) and (1.12)–(1.14)). Another property of

the "strange kinetic" is that this class of phenomena is inherent to many-particle cooperative systems. Such complex matter cannot be considered as a simple sum of elementary units but rather should be regarded as a whole system due to the interactions between the elementary components. In a wide sense the word "interaction" represents not only the interaction with some kind of physical far-ranging field (say an electromagnetic field) but can also mean a geometrical (or even a quantum) constraint, or other type of coupling. Consequently, it should be interesting and useful to find general origins to start, and then one can derive a whole variety of "strange kinetic" patterns.

Since "strange kinetic" is a property of macroscopic many-particle systems it can be analyzed in terms of statistical mechanics. The basic idea of statistical mechanics is the relaxation of the perturbed system to the equilibrium state. In general the distribution function $\rho(\boldsymbol{p},\boldsymbol{q};t)$ of a statistical ensemble depends on the generalized coordinates $\boldsymbol{q}$, momentum $\boldsymbol{p}$ and time t. However, in the equilibrium state it does not depend explicitly on time [111,127–130] and obeys the equation

$$\frac{\partial}{\partial t}\rho(\boldsymbol{p},\boldsymbol{q};t)=0. \tag{6.1}$$

The evolution of the distribution function to the equilibrium state is governed by the so-called Liouville equation (evolution equation)

$$\frac{\partial\rho(\boldsymbol{p},\boldsymbol{q};t)}{\partial t}=-i\mathscr{L}\rho(\boldsymbol{p},\boldsymbol{q};t), \tag{6.2}$$

where $\mathscr{L}$ is the Liouville operator. Thus, by virtue of (6.2) the evolution operator $\mathscr{L}$ determines the dynamical properties of the statistical system. The specific form of this operator is dependent on the Hamiltonian function H [111, 127–130] as

$$\mathscr{L}g=-\mathrm{i}\{H,g\}, \tag{6.3}$$

where $\{H,g\}$ are the Poisson brackets. In the classical statistical mechanics

$$\{H,g\}=\sum_k\left(\frac{\partial H}{\partial q_k}\frac{\partial g}{\partial p_k}-\frac{\partial H}{\partial p_k}\frac{\partial g}{\partial q_k}\right). \tag{6.4}$$

For the quantum mechanics the functions H, g become operators $\hat{H}$ and $\hat{g}$, and $\{\hat{H},\hat{g}\}$ obtains the commutator from $\{\hat{H},\hat{g}\}=2\pi/ih(\hat{H}\hat{g}-\hat{g}\hat{H})$, where h is the Plank constant.

Therefore, the consistent study of the many-particle system dynamics (in particular the "strange kinetic") should start by establishing the H and then solving the evolution equation (6.2). Unfortunately, examples of such calculations are very rare and valid for limited classes of model systems (like Ising model) since extended calculations. In particular, to the best of our knowledge, the relaxation patterns (1.10) and (1.12)–(1.14) still are not being derived this way.

In this section, we consider the problem from the opposite side. We will assume that (1.12)–(1.14) are given and try to guess what statistical properties leads to the "strange kinetic" behavior. Let us first examine the equilibrium state (6.1). The formal solution of (6.1) gives

$$\rho(\boldsymbol{p},\boldsymbol{q};t)=\text{const}. \tag{6.5}$$

Recently the new concept of fractional time evolution was introduced [93]. In addition to the usual equilibrium state (6.5), this concept leads to the possibility of the existence of an equilibrium state with power-law long-time behavior. In this case the infinitesimal generator of time evolution is proportional to the fractional time derivative operator ${}_0D_t^{\upsilon}$ (5.5) [93]. Obviously, the derivation order υ should be dependent on the properties of the cooperative system, although there is no clear understanding for the time being how υ depends on these properties.

Nevertheless, let us call the "fractional equilibrium state" the state of the statistical system that obeys the following:

$${}_0D_t^{\upsilon}\rho(\boldsymbol{p},\boldsymbol{q};t)=0. \tag{6.6}$$

We will discuss this state in relation to the recent approaches of the anomalous diffusion theory [27]. It is well known [111,127–129] that by virtue of the divergent form of Poisson brackets (6.4) the evolution of the distribution function $\rho(\boldsymbol{p},\boldsymbol{q};t)$ can be regarded as the flow of a fluid in the phase space. In this interpretation the Liouville equation (6.2) becomes analogous to the continuity equation for a fluid

$$\frac{\partial \rho}{\partial t} + \mathrm{div}(\rho \boldsymbol{v}) = 0, \tag{6.7}$$

where distribution function ρ is interpreted as the density of a fluid and $\boldsymbol{v}$ is its local velocity. Let us extend this analogy. The continuity equation accompanied by the relationship between the gradient of the fluid density and its flux (Darcy law for the liquid flow or Fourier law for heat flow for instance) [131,132]

$$\mathrm{grad}(\rho) = -\vartheta \rho \boldsymbol{v} \tag{6.8}$$

gives

$$\frac{\partial \rho}{\partial t} = \vartheta \Delta \rho, \tag{6.9}$$

where ϑ is the appropriate constant that characterizes permeability of the space and Δ is the Laplace differential operator. From a mathematical point of view Eq. (6.9) is analogous to the diffusion equation where ρ is regarded as the density of diffusing particles and ϑ is proportional to the appropriate diffusion coefficient.

It is well known that the diffusion equation can be obtained in two ways. The first is based on the equation of continuity and the relationship between the fluid density gradient of its flux (Eqs. (6.7)–(6.9)). The second way is the probabilistic approach developed from the theory of Brownian motion [27,110,111,127,128]. This approach does not appeal to the local differential equations like (6.7) and (6.8), but considers the probability of jumps between the sites of some lattice. There is an extension of this approach for the case when the lengths of the jumps as well as the waiting times between jumps are random. This is the so-called continuous time random walk (*CTRW*) scheme [27,133–135]. By applying different probability distribution functions for waiting time and jump length one can obtain different types of diffusion patterns [27]. In particular, if the characteristic waiting time diverges because of a long-tailed waiting time probability distribution function (proportional to $t^{-(1+\upsilon)}$), but the jump length variance is still kept finite, then diffusion equation (6.9) obtains a fractional derivation [27] instead of the first derivation on time on its left-hand side

$${}_0D_t^{\upsilon}\rho = \vartheta_{\upsilon}\Delta\rho. \tag{6.10}$$

Here the parameter ϑ_{υ} has a physical meaning similar to ϑ in (6.9), but with different a physical dimension. [2]

Now let us reiterate that diffusion equation (6.9) can be derived in two ways. Using a continuity equation and using the Brownian motion approach. By analogy one can imply that Eq. (6.10), a generalization of Eq. (6.9), can be derived not only in the framework of the *CTRW* scheme but also by using some analog of the continuity equation as well. The difference between Eqs. (6.9) and (6.10) is only in time derivation. Thus, the analog of continuity equation (6.7) that corresponds to the anomalous diffusion equation (6.10) is

$${}_0D_t^{\upsilon}\rho + \mathrm{div}(\rho \boldsymbol{v}_{\upsilon}) = 0. \tag{6.11}$$

Let us call it the "anomalous continuity equation". There are two main features that distinguish this equation from (6.7). The first is that (6.11) becomes non-local in time by virtue of the convolution form of the fractional derivation operator ${}_0D_t^{\upsilon}$. Second, in spite of the different physical dimension [m $s^{-\upsilon}$], the quantity $\boldsymbol{v}_{\upsilon}$ has a physical meaning similar to the local velocity $\boldsymbol{v}$.

Now let us return back to the Liouville equation. It was already mentioned that this equation can be regarded as a continuity equation. Thus, there is a possibility to establish an evolution equation not only in the usual form (6.2) but also based on the anomalous continuity equation (6.11) as well

$${}_0D_t^{\upsilon}\rho(\boldsymbol{p},\boldsymbol{q};t) = -i\mathscr{L}\rho(\boldsymbol{p},\boldsymbol{q};t). \tag{6.12}$$

This equation implies an equilibrium state in the (6.6) form.

Thus, the fractional equilibrium state (6.6) can be considered a consequence of the anomalous transport of phase points in the phase space that results in the anomalous continuity equation (6.11). Note that the usual form of evolution equation (6.2) is a direct consequence of the

[2] In the general case a term proportional to $\rho(t=0)$ should be added to the right-hand side of (6.10) but by choosing the appropriate initial conditions it can be subtracted. Thus, we will not discuss this term.

canonical Hamiltonian form of microscopic motion equations. Thus, the evolution of (6.12) implies that the microscopic equations of motion are not canonical. The actual form of these equations has not yet been investigated. However, there is great suspicion that in this case dissipative effects on the microscopic level become important.

If we assume factorization of time dependency in the distribution function, then the formal solution of (6.6) is

$$\rho_f(\boldsymbol{p},\boldsymbol{q};t) = \rho_f(\boldsymbol{p},\boldsymbol{q};\tau_f)\left(\frac{t}{\tau_f}\right)^{\upsilon-1}, \tag{6.13}$$

where $t \geqslant \tau_f$, $\rho_f(\boldsymbol{p},\boldsymbol{q};\tau_f)$ and τ_f depend on the initial conditions. Obviously, the assumption about factorization of time dependency for the distribution function is not universal. However, this type of factorization is justified when the equilibrium and non-equilibrium (in the ordinary sense) parts of distribution function $\rho(\boldsymbol{p},\boldsymbol{q};t)$ are orthogonal to each other in the phase space [130].

The interpretation of any distribution function as a probability density function in the phase space leads to the requirement

$$\int\int \rho(\boldsymbol{p},\boldsymbol{q};t)\frac{\mathrm{d}\boldsymbol{p}\,\mathrm{d}\boldsymbol{q}}{N!h^{3N}} = 1, \tag{6.14}$$

where $3N$ is the number of degrees of freedom. This normalization is based on the uncertainty relation that establishes the minimal phase cell as $\mathrm{d}p_k\mathrm{d}q_k \geqslant h$. Substitution of the solution (6.13) in (6.14) gives

$$\int\int \rho_f(\boldsymbol{p},\boldsymbol{q};t)\,\mathrm{d}\boldsymbol{p}\,\mathrm{d}\boldsymbol{q} = \frac{\Xi}{N!h^{3N}}\left(\frac{t}{\tau_\mathrm{f}}\right)^{\upsilon-1} = 1, \tag{6.15}$$

where

$$\Xi = \int\int \rho_f(\boldsymbol{p},\boldsymbol{q};\tau_f)\,\mathrm{d}\boldsymbol{p}\mathrm{d}\boldsymbol{q}$$

is a constant. Thus from (6.15) one can get

$$\frac{N!h^{3N}}{\Xi} = \left(\frac{t}{\tau_\mathrm{f}}\right)^{\upsilon-1}, \tag{6.16}$$

which for $\upsilon < 1$ indicates a decrease in the number of degrees of degrees of freedom.

From one point of view, (6.16) can be interpreted as a manifestation of the non-canonical nature of the microscopic motion equation and supports the idea of an impact of dissipative effects on the microscopic level (for time scale $t < \tau_f$). From another point of view (6.16) can be related to the "coarse graining" of the phase volume minimal cells. The concept of fractional evolution is the result of consequent acting of the averaging operator [93]. Each acting of the averaging operator is equal to the loss of information regarding the short-time mobility and is closely associated with the renormalization approach ideas [136].

A simple example of this "coarse graining" is that of two masses in the viscous media connected by a spring. The spring here represents an interaction between the microscopic particles while viscosity reflects the dissipative effects. Now let us discuss the situation when one mass is exposed by some mechanical perturbation with a wide spectrum (say the δ-impulse of force). In the beginning the motions of the masses are almost independent of each other. The viscosity effect then leads to a decay of the high-frequency modes of mobility and the motions of masses become more and more correlated. At the initial times, one should observe the motion of two centers of gravity while at the longer time interval it is enough to know the position of the joint center of gravity. Thus, the "coarse graining" effect leads to a reduction in the number of degrees of freedom.

The reduction of degrees of freedom can also be regarded as the transition from the non-correlated state to the state with long-range space correlations, and can be accompanied the phase transition. This is the reason the renormalization approach was used for the first time to describe the phase transition phenomena [111,128,136]. The theory of the phase transitions investigates the dependency of macroscopic physical quantities (like sample magnetization or polarization vectors) on the external parameter (like external fields or temperature) values. The changes of the degrees of freedom are the result of competition between external perturbations (say temperature) and internal interactions.

In contrast to the phase transitions in the fractional equilibrium state (6.6) the statistical

system looses degrees of freedom during evolution in time. The degrees of freedom, independent at the short-time limit, become dependent later due to the interactions (in the wide sense coupling, constraint, etc.) and dissipative effects.

The distribution function for the fractional equilibrium state (6.13) can be utilized to calculate the of macroscopic dipole correlation function (1.11). The statistical averaging designated $\langle\cdots\rangle$ in (1.11) is performed over the equilibrium ensemble (in the usual sense) with a distribution function that does not depend explicitly on time. If we regard the evolution of the *DCF* as a fractional equilibrium state (6.6), then by using properties of statistical averaging and the Liouville operator [129,130] we can transfer time dependence of the dynamic variable $\boldsymbol{M}(t)$ to time dependence of the distribution function $\rho_f(\boldsymbol{p},\boldsymbol{q};t)$. Thus, instead of $\langle\boldsymbol{M}(0)\boldsymbol{M}(t)\rangle$ in (1.11) we use $\langle\boldsymbol{M}(0)\boldsymbol{M}(0)\rangle_f$, where subscript f means that statistical averaging was performed with distribution function (6.13). In this case one can get

$$\begin{aligned}\phi(\mathrm{t}) &\cong \frac{\langle\boldsymbol{M}(0)\boldsymbol{M}(t)\rangle}{\langle\boldsymbol{M}(0)\boldsymbol{M}(0)\rangle} = \frac{\langle\boldsymbol{M}(0)\boldsymbol{M}(0)\rangle_f}{\langle\boldsymbol{M}(0)\boldsymbol{M}(0)\rangle} \\ &= \frac{\int\int \boldsymbol{M}(\boldsymbol{p},\boldsymbol{q};0)\boldsymbol{M}(\boldsymbol{p},\boldsymbol{q};0)\rho_f(\boldsymbol{p},\boldsymbol{q};t)\,\mathrm{d}\boldsymbol{p}\,\mathrm{d}\boldsymbol{q}}{\int\int \boldsymbol{M}(\boldsymbol{p},\boldsymbol{q};0)\boldsymbol{M}(\boldsymbol{p},\boldsymbol{q};0)\rho(\boldsymbol{p},\boldsymbol{q};0)\,\mathrm{d}\boldsymbol{p}\,\mathrm{d}\boldsymbol{q}} \\ &\sim \left(\frac{t}{\tau_\mathrm{f}}\right)^{v-1}, \quad t \geqslant \tau_\mathrm{f}. \end{aligned} \tag{6.17}$$

Thus, one can regard the power-law dependence of relaxation function (1.13) as a result of the fractional equilibrium state (6.6).

In order to understand the stretched exponential behavior of *DCF* (1.12) let us discuss Gibbs phase exponent $\eta_\mathrm{G} = -\ln\rho(\boldsymbol{p},\boldsymbol{q};t)$. This quantity plays a special role in statistical mechanics and relates to the entropy of the system. If Gibbs exponent obeys fractional evolution equation

$${}_0D_t^v\eta_G = 0, \tag{6.18}$$

then the distribution function is

$$\rho_\eta(\boldsymbol{p},\boldsymbol{q};t) = \rho_\eta(\boldsymbol{p},\boldsymbol{q};0)\exp\left(-\left(\frac{t}{\tau_\eta}\right)^{v-1}\right), \tag{6.19}$$

where $\rho_\eta(\boldsymbol{p},\boldsymbol{q};0)$ and τ_η depend on the initial conditions. A calculation analog to (6.17) shows that this distribution function leads to the *KWW* dependency of the *DCF*. Thus, in the framework of the fractional time evolution concept the power-law time dependence of the relaxation function behavior (1.13) and the stretched exponential relaxation (1.12) can be regarded as two different realizations: the fractal equilibrium state of the distribution function and the fractal evolution of Gibbs phase exponent.

A similar ideology can also be the basis of the relaxation pattern (1.14) when these two different types of fractal evolution simultaneously coexist for two subspaces $(\boldsymbol{p}_f,\boldsymbol{q}_f)$ and $(\boldsymbol{p}_\eta,\boldsymbol{q}_\eta)$ of the total statistical system phase space $(\boldsymbol{p},\boldsymbol{q})$. In this case the total distribution function $\rho_{f\eta}(\boldsymbol{p},\boldsymbol{q};t)$ is the product of two statistically independent distribution functions $\rho_f(\boldsymbol{p}_f,\boldsymbol{q}_f;t)$ and$\rho_\eta(\boldsymbol{p}_\eta,\boldsymbol{q}_\eta;t)$:

$$\begin{aligned}\rho_{f\eta}(\boldsymbol{p},\boldsymbol{q};t) = \rho_\eta(\boldsymbol{p}_\eta,\boldsymbol{q}_\eta;0)\rho_f(\boldsymbol{p}_f,\boldsymbol{q}_f;\tau_f)\left(\frac{t}{\tau_f}\right)^{v-1} \\ \times\exp\left(-\left(\frac{t}{\tau_\eta}\right)^{v-1}\right),\end{aligned} \tag{6.20}$$

that can be related to the relaxation pattern (1.14).

The relaxation law (6.20) has been observed in the case of dynamic percolation in ionic microemulsions (see Section 2). Below the percolation threshold, the relaxation process is provided by two types of mobility: mobility of the pre-percolation clusters and mobility of the charge carriers inside these clusters. The first type of mobility is governed by the power law (1.13) while the second type exhibits stretched exponential behavior (1.12) [54]. Thus, there are two subspaces of degrees of freedom: the first is related to the mobility of pre-percolation clusters as a whole and the second reflects the mobility inside the clusters. Approaching the percolation threshold pre-percolation clusters grow and become an infinite (or very large for a real finite size system) percolation cluster at the threshold. At this point mobility of the cluster is impossible, as first subspace of degrees of freedom disappear and the relaxation function obtains the stretched exponential pattern (1.12). Far from the percolation, one finds the opposite situation. The pre-percolation clusters are

small, second subspace degrees of freedom are not yet developed and the relaxation function obeys the power law (1.13).

Obviously, the arguments represented in this section are not rigorous. They are the hints rather than the proofs. Nevertheless, we discuss them here for the following reasons. We have exposed quite a few different models of "strange kinetic" phenomena and we have presented a few of them above (see Sections 2–5). However, in our opinion, there is no unified ideology yet that can explain the backgrounds of the "strange kinetics". Thus, we have tried not to answer, but rather raise questions and present new points of view on the problem.

Acknowledgements

The authors would like to express their deep appreciation to Mrs. A. Gutina and Mrs. E. Axelrod for their help in preparation of figures and data treatment as well as Prof. A. Sa'ar and Dr. V. Arkhipov for comprehensive discussions.

References

[1] M.F. Shlesinger, G.M. Zaslavsky, J. Klafter, Nature 363 (1993) 31.
[2] A. Schönhals, F. Kremer, A. Hofmann, E.W. Fischer, E. Scholosser, Phys. Rev. Lett. 70 (1993) 3459.
[3] P. Lunkenheimer, A. Pimenov, M. Dressel, Yu.G. Goncharov, R. Böhmer, A. Loidl, Phys. Rev. Lett. 77 (1996) 318.
[4] U. Scheider, P. Lunkenheimer, R. Brand, A. Loidl, J. Non-Cryst. Solids 235–237 (1998) 173.
[5] H. Förhlich, Theory of Dielectrics, Clarendon Press, Oxford, 1958.
[6] C.J.F. Böttcher, P. Bordewijk, Theory of Electric Polarization, vol. 2, second ed., Elsevier, Amsterdam, 1992.
[7] N.E. Hill, W.E. Yaughan, A.H. Price, M. Davis, Dielectric Properties and Molecular Behavior, Van Nostrand, London, 1969.
[8] B.K.P. Scaife, Principles of Dielectrics, Oxford University Press, Oxford, 1989.
[9] A.N. Tikhonov, V.Y. Arsenin, Solutions of Ill-Posed Problems, Wiley, New York, 1977.
[10] H. Schäfer, E. Sternin, R. Stannarius, M. Arndt, F. Kremer, Phys. Rev. Lett. 76 (1996) 2177.
[11] A. Bello, E. Laredo, M. Grimau, Phys. Rev. B 60 (1999) 12764.
[12] S. Havriliak, S. Negami, J. Polymer Science: Part C 14 (1966) 99.
[13] K.S. Cole, R.H. Cole, J. Chem. Phys. 9 (1941) 341.
[14] D.W. Davidson, R.H. Cole, J. Chem. Phys. 19 (1951) 1484.
[15] A.K. Jonscher, Dielectric Relaxation in Solids, Chelsea Dielectric Press, London, 1983.
[16] A.K. Jonscher, Universal Relaxation Law, Chelsea Dielectric Press, London, 1996.
[17] J.C. Dyre, T.B. Schrøder, Rev. Mod. Phys. 72 (2000) 873.
[18] N.F. Mott, E.A. Davis, Electronic Processes in Non-Crystalline Materials, Clarendon Press, Oxford, 1971.
[19] R.R. Nigmatullin, Ya.E. Ryabov, Phys. Solid State 39 (1997) 87.
[20] L. Nivanen, R. Nigmatullin, A. LeMehaute, Le Temps Irreversible a Geometry Fractale, Hermez, Paris, 1998.
[21] S. Alexander, J. Bernasconi, W.R. Schneider, R. Orbach, Rev. Mod. Phys. 53 (1981) 175.
[22] M. Ben-Chorin, F. Moller, F. Koch, W. Schirmacher, M. Eberhard, Phys. Rev. B 51 (1995) 2199.
[23] G. Williams, Chem. Rev. 72 (1972) 55.
[24] R.H. Cole, in: Molecular Liquids NATO ASI Ser. C, vol. 135, 1984, p. 59.
[25] R. Kohlrausch, Ann. Phys. (Leipzig) 12 (1847) 393.
[26] G. Williams, D.C. Watts, Trans. Faraday Soc. 66 (1970) 80.
[27] R. Metzler, J. Klafter, Phys. Rep. 339 (2000) 1.
[28] A. Blumen, J. Klafter, G. Zumofen, in: I. Zschokke (Ed.), Optical Spectroscopy of Glasses, Reidel, Dordrecht, The Netherlands, 1986, p. 199.
[29] G.H. Weiss, Aspects and Applications of the Random Walk, North-Holland, Amsterdam, 1994.
[30] E. Barkai, R. Metzler, J. Klafter, Phys. Rev. E 61 (2000) 132.
[31] T. Zavada, N. Südland, R. Kimmich, T.F. Nonnenmacher, Phys. Rev. E 60 (1999) 1292.
[32] T. Wadayama, S. Yamamoto, A. Hatta, Appl. Phys. Lett. 65 (1994) 1653.
[33] V. Degiorgio, R. Piazza, F. Mantegazza, T. Bellini, J. Phys.: Condens. Matter 2 (1990) SA69.
[34] J.E. Martin, D. Adolf, J.P. Wilcoxon, Phys. Rev. A 39 (1989) 1325.
[35] F. Alvarez, A. Alegría, J. Colmenero, Phys. Rev. B 44 (1991) 7306.
[36] S.E. Friberg, Microemulsions: Structure and Dynamics, CRC Press, Boca Raton, FL, 1987.
[37] B. Lindman (Ed.), Surfactants, Adsorption, Surface Spectroscopy and Disperse Systems, Steinkopff, Darmstadt, 1985.
[38] D. Langevin, Annu. Rev. Phys. Chem. 43 (1992) 341.
[39] J. Sjöblom, R. Lindberg, S.E. Friberg, Adv. Colloid Interface Sci. 95 (1996) 125.
[40] U. Olsson, K. Shinoda, B. Lindman, J. Phys. Chem. 90 (1986) 4083.
[41] P.G. DeGennes, C. Touplin, J. Phys. Chem. 86 (1982) 2294.
[42] M.A. Dijk, G. Casteleijn, J.G.H. Joosten, Y.K. Levine, J. Chem. Phys. 85 (1986) 626.
[43] Yu. Feldman, N. Kozlovich, I. Nir, N. Garti, Phys. Rev. E 51 (1995) 478.

[44] Yu. Feldman, N. Kozlovich, Y. Alexandrov, R. Nigmatullin, Ya. Ryabov, Phys. Rev. E 54 (1996) 5420.
[45] C. Cametti, P. Codastefano, P. Tartaglia, S. Chen, J. Rouch, Phys. Rev. A 45 (1992) R5358.
[46] F. Bordi, C. Cametti, J. Rouch, F. Sciortino, P. Tartaglia, J. Phys.: Condens. Matter 19 (1996) 8.
[47] C. Boned, J. Peyrelasse, Z. Saidi, Phys. Rev. E 47 (1993) 468.
[48] A. Ponton, T.K. Bose, G. Delbos, J. Chem. Phys. 94 (1991) 6879.
[49] Yu. Feldman, N. Kozlovich, I. Nir, N. Garti, V. Archipov, Z. Idiyatullin, Y. Zuev, V. Fedotov, J. Phys. Chem. 100 (1996) 3745.
[50] A.L.R. Bug, S.A. Safran, G.S. Grest, I. Webman, Phys. Rev. Lett. 55 (1985) 1896.
[51] N. Kozlovich, A. Puzenko, Yu. Alexandrov, Yu. Feldman, Colloids and Surfaces A 140 (1998) 299.
[52] G. Grest, I. Webman, S. Safran, A. Bug, Phys. Rev. A 33 (1986) 2842.
[53] C. Cametti, P. Codastefano, A. Di Biasio, P. Tartaglia, S. Chen, Phys. Rev. A 40 (1989) 1962.
[54] D. Stauffer, A. Aharony, Introduction to Percolation Theory, revised second ed., Taylor & Francis, London, 1994.
[55] J. Feder, Fractals, Plenum Press, New York, 1988.
[56] A. Bunde, S. Havlin (Eds.), Fractals and Disordered Systems, Springer, Berlin, 1996.
[57] A. Puzenko, N. Kozlovich, Yu. Feldman, Phys. Rev. E (submitted).
[58] Yu. Feldman, A. Andrianov, E. Polygalov, G. Romanychev, I. Ermolina, Yu. Zuev, B. Milgotin, Rev. Sci. Instrum. 67 (1996) 3208.
[59] E. Rysiakiewicz-Pasek, K. Marczuk, J. Porous Materials 3 (1996) 17.
[60] A. Gutina, E. Axelrod, A. Puzenko, E. Rysiakiewicz-Pasek, N. Kozlovich, Yu. Feldman, J. Non-Cryst. Solids 235–237 (1998) 302.
[61] A. Puzenko, N. Kozlovich, A. Gutina, Yu. Feldman, Phys. Rev. B 60 (1999) 14348.
[62] Ya. Ryabov, A. Gutina, V. Arkhipov, Yu. Feldman, J. Phys. Chem. B 105 (2001) 1845.
[63] A. Gutina, E. Rysiakiewicz-Pasek, T. Antropova, Yu. Feldman, Microporous and Mesoporous Materials (submitted).
[64] J. Klafter, A. Blumen, Chem. Phys. Lett. 119 (1985) 377.
[65] J. Klafter, M.F. Shlesinger, Proc. Natl. Acad. Sci. USA 83 (1986) 848.
[66] U. Even, K. Rademann, J. Jortner, N. Manor, R. Reisfeld, Phys. Rev. Lett. 52 (1984) 2164.
[67] U. Even, K. Rademann, J. Jortner, N. Manor, R. Reisfeld, Phys. Rev. Lett. 58 (1987) 285.
[68] R. Hilfer, in: I. Prigogine, A. Rice (Eds.), Advances in Chemical Physics, vol. XCII, Wiley, New York, 1996, p. 299.
[69] R.R. Nigmatullin, Phys. Stat. Sol. 153 (1989) 49.
[70] W.D. Dozier, J.M. Drake, J. Klafter, Phys. Rev. Lett. 56 (1986) 197.
[71] E. Axelrod, A. Givant, J. Shappir, Yu. Feldman, A. Sa'ar, J. Non-Cryst. Solids (in press).
[72] L.T. Canham, Appl. Phys. Lett. 57 (1990) 1046.
[73] A.G. Cullis, L.T. Canham, P.D.J. Calcolt, J. Appl. Phys. 82 (1997) 909.
[74] L. Canham (Ed.), Properties of Porous Silicon, Emis data reviews series, vol. 18, Inspec Publication, London, 1997.
[75] O. Bisi, S. Ossicini, L. Pavesi, Surf. Sci. Rep. 38 (2000) 1.
[76] A. Gutina, Ya. Haruvy, I. Gilath, E. Axelrod, N. Kozlovich, Yu. Feldman, J. Phys. Chem. 103 (1999) 5454.
[77] G. Øye, E. Axelrod, Yu. Feldman, J. Söjblom, M. Stöcker, Colloid Polymer Sci. 278 (2000) 517.
[78] T. Saraidaro, E. Axelrod, Yu. Feldman, R. Reisfeld, Chem. Phys. Lett. 324 (2000) 7.
[79] L. Lubianiker, I. Balberg, Phys. Rev. Lett. 78 (1997) 2433.
[80] J. Kocka, J. Oswald, A. Fejfar, R. Sedlacik, V. Zelezny, Ho The-Ha, I. Pelant, Thin Solid Films 276 (1996) 187.
[81] E. Axelrod, A. Givant, J. Shappir, Yu. Feldman, A. Sa'ar, Phys. Rev. B 65 (2001) 165249.
[82] I. Webman, Phys. Rev. Lett. 47 (1981) 1496.
[83] T. Odagaki, M. Lax, Phys. Rev. B 24 (1981) 5284.
[84] J. Kakalios, R.A. Street, W.B. Jackson, Phys. Rev. Lett. 59 (1987) 1037.
[85] E.W. Fisher, E. Donth, W. Steffen, Phys. Rev. Lett. 68 (1992) 2344.
[86] J. Colmenero, A. Alegía, A. Arbe, B. Frick, Phys. Rev. Lett. 69 (1992) 478.
[87] W. Götze, L. Sjögren, Rep. Prog. Phys. 55 (1992) 241.
[88] M. Salomon, M.Z. Xu, E.M. Eyring, S. Petrucci, J. Phys. Chem. 98 (1994) 8234.
[89] N. Shinyashiki, S. Yagihara, I. Arita, S. Mashimo, J. Phys. Chem. B 102 (1998) 3249.
[90] P.K. Choi, R. Tanimoto, Jpn. J. Appl. Phys. 39 (2000) 2898.
[91] M. Mierzwa, G. Floudas, P. Štepánek, G. Wegner, Phys. Rev. B 62 (2000) 14012.
[92] Ya.E. Ryabov, Ph.D. Thesis, Kazan State University, Russia, 1996.
[93] R. Hilfer (Ed.), Applications of Fractional Calculus in Physics, World Scientific, London, 2000.
[94] I. Ermolina, G. Smith, Ya. Ryabov, A. Puzenko, Yu. Polevaya, R. Nigmatullin, Yu. Feldman, J. Phys. Chem. B 104 (2000) 1373.
[95] S. Fujiwara, F. Yonezwara, Phys. Rev. E 51 (1995) 2277.
[96] S. Gomi, F. Yonezwara, Phys. Rev. Lett. 74 (1995) 4125.
[97] V. Halpern, Phys. Rev. B 56 (1997) R11 377.
[98] V. Raicu, Phys. Rev. E 60 (1999) 4677.
[99] A. Zetsche, F. Kremer, W. Jung, H. Schulze, Polymer 31 (1990) 336.
[100] G. Katana, F. Kremer, E.W. Fisher, R. Plaetschke, Macromolecules 26 (1993) 3075.
[101] A. Schönhals, F. Kremer, J. Non-Cryst. Solids 172–174 (1994) 336.
[102] G. Katana, E.W. Fischer, Th. Hack, V. Abetz, F. Kremer, Macromolecules 28 (1995) 2714.
[103] K. Oldham, J. Spanier, The Fractional Calculus, Academic Press, New York, 1974.

[104] K. Miller, B. Ross, An Introduction to the Fractional Calculus and Fractional Differential Equations, Wiley, New York, 1993.
[105] I.M. Sokolov, Phys. Rev. E 63 (2001) 011104.
[106] H. Mori, Prog. Theor. Phys. 33 (1965) 423.
[107] H. Mori, Prog. Theor. Phys. 34 (1965) 399.
[108] J.A. Korn, T.M. Korn, Mathematical Handbook, McGraw-Hill, New York, 1968.
[109] K. Weron, A. Klauzer, Ferroelectrics 236 (2000) 59.
[110] A. Einstein, Ann. Phys. (Leipzig) 322 (1905) 549.
[111] P.K. Pathria, Statistical Mechanics, Pergamon Press, Oxford, 1972.
[112] J.B. Hasted, in: F. Franks (Ed.), Water, A Comprehensive Treaties, Plenum Press, New York, 1972, p. 255.
[113] U. Kaatze, J. Chem. Eng. Data 34 (1989) 371.
[114] Ya. Ryabov, Yu. Feldman, N. Shinyashki, S. Yagihara, J. Chem. Phys. 16 (2002) 8610.
[115] J. Barthel, K. Bachhuber, R. Buchner, H. Hetzenauer, Chem. Phys. Lett. 165 (1990) 369.
[116] U. Kaatze, J. Mol. Liq. 56 (1993) 95.
[117] R. Buchner, J. Barthel, J. Stauber, Chem. Phys. Lett. 306 (1999) 57.
[118] C. Ronne, P. Astrad, S.R. Keiding, Phys. Rev. Lett. 82 (1999) 2888.
[119] D. Eisenberg, W. Kauzman, The Structure and Properties of Water, Clarendon Press, Oxford, 1969.
[120] H. Nuriel, N. Kozlovich, Yu. Feldman, G. Marom, Composites: Part A 31 (2000) 69.
[121] P.G. DeGennes, J. Chem. Phys. 55 (1971) 572.
[122] W.W. Graessley, J. Polym. Sci.: Polym. Phys. 18 (1980) 27.
[123] F. Joabsson, M. Nyden, K. Thuresson, Macromolecules 33 (2000) 6772.
[124] J.E.M. Snaar, P. Robyr, R. Bowtell, Mag. Res. Im. 16 (1998) 587.
[125] P. Gribbon, B.C. Heng, T.E. Hardingham, Biophys. J. 77 (1999) 2210.
[126] E. Donth, J. Non-Cryst. Solids 131–133 (1991) 204.
[127] L.D. Landau, E.M. Lifshitz, Statistical Mechanics, Pergamon Press, Oxford, 1980.
[128] Sh.K. Ma, Statistical Mechanics, World Scientific, Singapore, 1985.
[129] D.N. Zubarev, Nonequilibrium Statistical Thermodynamics, Consultant Bureau, New York, 1974.
[130] R.W. Zwanzig, in: W.E. Brittin, B.W. Downs, J. Downs (Eds.), Lectures in Theoretical Physics, vol. III, Interscience, New York, 1961, p. 106.
[131] H. Darcy, Fontanies Publiques de la Ville de Dijon, Libraire des Corps Imperiaux des Ponts et Chausses et des Mines, Paris, 1856.
[132] J.B.J. Fourier, Théorie Analytique de la Chaleur, Firmin Didot, Père et Fils, Paris, 1822.
[133] E.W. Montroll, G.H. Weiss, J. Math. Phys. 6 (1965) 167.
[134] H. Scher, M. Lax, Phys. Rev. B 7 (1973) 4491.
[135] H. Scher, M. Lax, Phys. Rev. B 7 (1973) 4502.
[136] K.G. Wilson, J. Kogut, Phys. Rep. 2 (1974) 75.